

OPTIMAL ENERGY-CONSERVING DISCONTINUOUS GALERKIN METHODS FOR LINEAR SYMMETRIC HYPERBOLIC SYSTEMS

GUOSHENG FU AND CHI-WANG SHU

ABSTRACT. We propose energy-conserving discontinuous Galerkin (DG) methods for symmetric linear hyperbolic systems on general unstructured meshes. Optimal a priori error estimates of order $k + 1$ are obtained for the semi-discrete scheme in one dimension, and in multi-dimensions on Cartesian meshes when tensor-product polynomials of degree k are used. A high-order energy-conserving Lax-Wendroff time discretization is also presented.

Extensive numerical results in one dimension, and two dimensions on both rectangular and triangular meshes are presented to support the theoretical findings and to assess the new methods. One particular method (with the doubling of unknowns) is found to be optimally convergent on triangular meshes for all the examples considered in this paper. The method is also compared with the classical (dissipative) upwinding DG method and (conservative) DG method with a central flux. It is numerically observed for the new method to have a superior performance for long-time simulations.

1. INTRODUCTION

Wave propagation problems arise in science, engineering and industry, and they are significant to geoscience, petroleum engineering, telecommunication, and the defense industry (see [11, 17] and the references therein). Efficient and accurate numerical methods to solve wave propagation problems are of fundamental importance to these applications. Experience reveals that energy conserving numerical methods, which conserve the discrete approximation of energy, are favorable because they are able to maintain the phase and shape of the waves accurately, especially for long time simulation.

A vast amount of literature can be found on the numerical approximation of wave problems modeled by linear hyperbolic systems. All types of numerical methods, including finite difference, finite element, finite volume and spectral methods have their proponents. Here, we will confine our attention in finite element methods, in particular, discontinuous Galerkin (DG) methods. The DG methods, c.f. [8], belong to a class of finite element methods using discontinuous piecewise polynomial spaces for both the numerical solution and the test functions. They allow arbitrarily unstructured meshes, and have compact stencils. Moreover, they easily accommodate arbitrary h-p adaptivity.

2010 *Mathematics Subject Classification.* Primary 65M60, 65M12, 65M15.

Key words and phrases. discontinuous Galerkin method, energy conserving, hyperbolic system.

The research of the second author was supported by ARO grant W911NF-15-1-0226 and NSF grant DMS-1719410.

Various DG methods can be applied to solve linear hyperbolic systems. We mention the classical Runge-Kutta DG method of Cockburn and Shu [10], the nodal DG method of Hesthaven and Warburton [16], the space-time DG method of Falk and Richter [12] and Monk and Richter [23]. All these DG methods use approximate/exact Riemann solvers to define the numerical flux, and are dissipative by design.

A suboptimal energy-conserving DG method using central fluxes, has been presented by Fezoui et. al. in [13] for the Maxwells equations. Chung and Engquist [6] have proposed an optimal, energy conserving DG method for the acoustic wave equation on staggered grids. More recently, Xing et. al. [5] proposed an optimal, energy conserving DG method using alternating fluxes for the acoustic wave equation on Cartesian grids. These DG methods do not rely on approximate/exact Riemann solvers to define the numerical flux.

Our work can be considered as a continuation of [5] on the search for optimal, energy-conserving DG methods for general linear symmetric hyperbolic systems. We propose an energy-conserving DG method for linear symmetric hyperbolic systems on general unstructured meshes. The method on Cartesian meshes is identical to the DG method using alternating fluxes [5] for the acoustic wave equation considered therein. They may be different on general triangular meshes. We prove optimal convergence of the proposed semi-discrete DG method in one-space dimension. In particular, we present, for the first time, an optimal, energy-conserving DG method for the scalar advection equation on general non-uniform meshes in one dimension. Similar to [5], the semi-discrete DG method can be also proven to be optimally convergent in multi-dimensions on Cartesian meshes, essentially using the superconvergence result of Lesaint and Raviart [18] for the tensor-product Gauss-Radau projection. On the other hand, on general triangular meshes, we are only able to prove a suboptimal convergence for the proposed method using a standard L^2 -projection type analysis. However, in all our numerical results on unstructured triangular meshes presented in this paper, including the scalar advection equation, the acoustic equations, and the equations for elastodynamics, the method is observed to be optimally convergent. A theoretical study of the convergence property of the proposed method on triangular meshes consists of our ongoing work.

The rest of the paper is organized as follows. In Section 2, we first present and analyze the semi-discrete energy-conserving DG method for linear symmetric hyperbolic systems in one dimension. We also present the high-order energy-conserving Lax-Wendroff time discretization. In Section 3, the method is extended to multi-dimensions. Numerical results are reported in Section 4. Finally, we conclude in Section 5.

2. ENERGY-CONSERVING DG METHODS FOR THE ONE-DIMENSIONAL CASE

In this section, we present and analyze the energy-conserving DG methods for linear symmetric hyperbolic systems in one dimension. The extension to the multidimensional case will be consider in the next section.

2.1. Notation and definitions in the one-dimensional case. In this subsection, we shall first introduce some notation and definitions in the one-dimensional case, which will be used throughout this section.

2.1.1. *The meshes.* Let us denote by \mathcal{I}_h a tessellation of the computational interval $I = [0, 1]$, consisting of cells $I_j = (x_{j-\frac{1}{2}}, x_{j+\frac{1}{2}})$ with $1 \leq j \leq N$, where

$$0 = x_{\frac{1}{2}} < x_{\frac{3}{2}} < \cdots < x_{N+\frac{1}{2}} = 1.$$

The following standard notation of DG methods will be used. Denote $x_j = (x_{j-\frac{1}{2}} + x_{j+\frac{1}{2}})/2$, $h_j = x_{j+\frac{1}{2}} - x_{j-\frac{1}{2}}$, $h = \max_j h_j$, and $\rho = \min_j h_j$. The mesh is assumed to be regular in the sense that h/ρ is always bounded during mesh refinements, namely, there exists a positive constant γ such that $\gamma h \leq \rho \leq h$. We denote by $p_{j+\frac{1}{2}}^-$ and $p_{j+\frac{1}{2}}^+$ the values of p at the discontinuity point $x_{j+\frac{1}{2}}$, from the left cell, I_j , and from the right cell, I_{j+1} , respectively. In what follows, we employ $[[p]] = p^+ - p^-$ and $\{\{p\}\} = \frac{1}{2}(p^+ + p^-)$ to represent the jump and the mean value of p at each element boundary point. The following discontinuous piecewise polynomials space is chosen as the finite element space:

$$V_h \equiv V_h^k = \{v \in L^2(I) : v|_{I_j} \in P^k(I_j), j = 1, \dots, N\}, \quad (2.1)$$

where $P^k(I_j)$ denotes the set of polynomials of degree up to $k \geq 0$ defined on the cell I_j .

2.1.2. *Function spaces and norms.* Denote $H^1(I)$ as the space of L^2 functions on I whose derivative is also an L^2 function. Denote $\|\cdot\|_{I_j}$ the standard L^2 -norm on the cell I_j , and $\|\cdot\|_I$ the L^2 -norm on the whole interval.

2.2. Energy-conserving DG methods for linear symmetric hyperbolic systems. We first start with a general form of energy-conserving DG method for the following linear symmetric hyperbolic system:

$$\mathbf{B}_0 \mathbf{u}_t + \mathbf{B}_1 \mathbf{u}_x = 0, \quad (x, t) \in I \times (0, T], \quad (2.2)$$

with initial condition $\mathbf{u}(x, 0) = \mathbf{u}_0(x)$, and periodic boundary condition. Here the unknown is $\mathbf{u} : I \times (0, T] \rightarrow \mathbb{R}^m$, and $\mathbf{u} = (u^1, \dots, u^m)$. The matrix $\mathbf{B}_0 : I \rightarrow \mathbb{R}^{m \times m}$ is a diagonal matrix with positive, piecewise constant diagonal entries, and $\mathbf{B}_1 \in \mathbb{R}^{m \times m}$ is a *symmetric constant coefficient* matrix.

The semi-discrete DG method for (2.2) reads as follows. Find, for any time $t \in (0, T]$, the unique function $\mathbf{u}_h = \mathbf{u}_h(t) \in [V_h^k]^m$ such that

$$\int_{I_j} \mathbf{B}_0(\mathbf{u}_h)_t \cdot \mathbf{v}_h \, dx - \int_{I_j} \mathbf{B}_1 \mathbf{u}_h \cdot (\mathbf{v}_h)_x \, dx + \widehat{\mathbf{B}}_1 \mathbf{u}_h \cdot \mathbf{v}_h^-|_{j+\frac{1}{2}} - \widehat{\mathbf{B}}_1 \mathbf{u}_h \cdot \mathbf{v}_h^+|_{j-\frac{1}{2}} = 0, \quad (2.3a)$$

holds for all $\mathbf{v}_h \in [V_h^k]^m$ and all $j = 1, \dots, N$. The *consistent* numerical fluxes $\widehat{\mathbf{B}}_1 \mathbf{u}_h$ is single-valued on the cell boundaries $x_{j-1/2}$, and it is given by the following form

$$\widehat{\mathbf{B}}_1 \mathbf{u}_h|_{j-\frac{1}{2}} = \mathbf{B}_1 \{\{\mathbf{u}_h\}\} + \mathbf{R}_{j-\frac{1}{2}} \llbracket \mathbf{u}_h \rrbracket, \quad (2.3b)$$

where $\mathbf{R}_{j-\frac{1}{2}} \in \mathbb{R}^{m \times m}$ is a, yet to be determined, *stabilization* matrix at $x_{j-\frac{1}{2}}$.

Remark 2.1 (The stabilization matrix $\mathbf{R}_{j-\frac{1}{2}}$). Since the matrices $\mathbf{R}_{j-\frac{1}{2}}$ do not depend on the numerical solution \mathbf{u}_h , the semi-discrete DG scheme (2.3) with the numerical flux (2.3b) is a linear scheme. In the most general form of a *local* numerical flux, the stabilization $\mathbf{R}_{j-\frac{1}{2}}$ may depend on \mathbf{u}_h^\pm at the interface $x_{j-\frac{1}{2}}$, which will leads to a nonlinear scheme for the linear equation (2.2). We always consider

the linear numerical flux (2.3b) in this work, as we do not see any advantage of a nonlinear scheme for the equation (2.2).

Summing the equations (2.3) for all j , and using the periodic boundary condition, we have

$$\sum_{j=1}^N \left(\int_{I_j} \mathbf{B}_0(\mathbf{u}_h)_t \cdot \mathbf{v}_h dx - \int_{I_j} \mathbf{B}_1 \mathbf{u}_h \cdot (\mathbf{v}_h)_x dx - \widehat{\mathbf{B}}_1 \mathbf{u}_h \cdot \llbracket \mathbf{v}_h \rrbracket \Big|_{j-\frac{1}{2}} \right) = 0, \quad (2.4)$$

As is well-known, the linear symmetric hyperbolic system (2.2) admits an important conserved quantity – the energy,

$$E(t) = \int_I (\mathbf{B}_0 \mathbf{u}(t)) \cdot \mathbf{u}(t) dx,$$

that is, $E(t) = E(0)$ for all $t > 0$. Experiences show that schemes conserving the discrete analogs of energy often produce approximations that behave better for long time simulation. We are particularly interested in deriving optimally-convergent, and energy-conserving DG methods. We call the semi-discrete DG method an energy-conserving DG method if the discrete energy

$$E_h(t) := \int_I (\mathbf{B}_0 \mathbf{u}_h \cdot \mathbf{u}_h) dx \quad (2.5)$$

is conserved for all time.

The following theorem provide a sufficient and necessary condition for energy conservation of the DG methods (2.3).

Theorem 2.2. *The (continuous-in-time) energy $E_h(t)$ (2.5) is conserved by the semi-discrete DG scheme (2.3) for any initial condition $\mathbf{u}_0(x)$, for all time $t > 0$ if and only if the stabilization matrix $\mathbf{R}_{j-1/2}$ is anti-symmetric for all j .*

Proof. Taking $\mathbf{v}_h = \mathbf{u}_h$ in the scheme (2.4), and using the definition of the numerical flux (2.3b), we have

$$\begin{aligned} \int_I \mathbf{B}_0(\mathbf{u}_h)_t \cdot \mathbf{u}_h dx &= \sum_{j=1}^N \int_{I_j} \mathbf{B}_1 \mathbf{u}_h \cdot (\mathbf{u}_h)_x dx \\ &+ \sum_{j=1}^N (\mathbf{B}_1 \{\!\!\{ \mathbf{u}_h \}\!\!\} + \mathbf{R}_{j-\frac{1}{2}} \llbracket \mathbf{u}_h \rrbracket) \cdot \llbracket \mathbf{u}_h \rrbracket \Big|_{j-\frac{1}{2}}. \end{aligned} \quad (2.6)$$

By symmetry of \mathbf{B}_1 , we have $\mathbf{B}_1 \mathbf{u}_h \cdot (\mathbf{u}_h)_x = \frac{1}{2} (\mathbf{B}_1 \mathbf{u}_h \cdot \mathbf{u}_h)_x$. Applying integration by parts of each of the above integral on the right hand side, and using the periodic boundary condition, the right side of (2.6) can be simplifies as

$$\sum_{j=1}^N \left(\mathbf{B}_1 \{\!\!\{ \mathbf{u}_h \}\!\!\} + \mathbf{R}_{j-\frac{1}{2}} \llbracket \mathbf{u}_h \rrbracket \right) \cdot \llbracket \mathbf{u}_h \rrbracket - \left(\frac{1}{2} \mathbf{B}_1 \mathbf{u}_h^+ \cdot \mathbf{u}_h^+ - \frac{1}{2} \mathbf{B}_1 \mathbf{u}_h^- \cdot \mathbf{u}_h^- \right) \Big|_{j-\frac{1}{2}}.$$

A simple calculation yields

$$\mathbf{B}_1 \{\!\!\{ \mathbf{u}_h \}\!\!\} \cdot \llbracket \mathbf{u}_h \rrbracket - \left(\frac{1}{2} \mathbf{B}_1 \mathbf{u}_h^+ \cdot \mathbf{u}_h^+ - \frac{1}{2} \mathbf{B}_1 \mathbf{u}_h^- \cdot \mathbf{u}_h^- \right) = 0.$$

Combining this with (2.6) and (2.5), we have

$$\frac{d}{dt} \frac{1}{2} E_h(t) = \sum_{j=1}^N \mathbf{R}_{j-\frac{1}{2}} \llbracket \mathbf{u}_h \rrbracket \cdot \llbracket \mathbf{u}_h \rrbracket \Big|_{j-\frac{1}{2}}. \quad (2.7)$$

Requiring $\frac{d}{dt}E_h(t) = 0$ for all time, for any initial condition $\mathbf{u}_h(0)$ simply implies that

$$\mathbf{R}_{j-\frac{1}{2}} \mathbf{v} \cdot \mathbf{v} = 0 \quad \forall \mathbf{v} \in \mathbb{R}^m, \quad \forall j.$$

Hence, $\mathbf{R}_{j-\frac{1}{2}}$ must be an anti-symmetric matrix for all j . \square

Remark 2.3 (Scalar case, $m = 1$). Theorem 2.2 implies that, in the case $m = 1$, there exists only *one* energy-conserving DG method of the form (2.3), where $\mathbf{R}_{j-\frac{1}{2}} \equiv 0$ for all j , and the resulting numerical flux is nothing but the central flux.

It is well-known that DG methods with a central flux provide suboptimal L^2 -convergence order of k when polynomials of degree k is used, with the exception that optimal convergence order of $k + 1$ can be proven under the stringent assumption that mesh is uniform and polynomial degree k is even, c.f. [9]. Violating either of these assumptions results in suboptimal convergence. While there seems no hope to obtain optimal-convergent, energy-conserving DG methods for the scalar advection equation on nonuniform mesh, we show in the next subsection, that by simply doubling the number of unknowns, we can obtain an optimal-convergent, energy-conserving DG method on general nonuniform meshes.

2.3. Optimal energy-conserving DG method for advection. In this subsection, we consider the following advection equation

$$u_t + c u_x = 0, \quad (x, t) \in I \times (0, T], \quad (2.8)$$

with a smooth periodic initial condition $u(x, 0) = u_0(x)$ for $x \in I$. Again, we assume periodic boundary condition for simplicity. Here we assume the speed c is a piecewise positive constant on the mesh. Note that the equation (2.8) can be recast into the general form (2.2) with $\mathbf{B}_0 = c^{-1}$, $\mathbf{B}_1 = 1$.

To derive the energy-conserving DG method for the advection equation (2.8), we shall first double the unknowns by introducing an auxiliary *zero* function $\phi(x, t) = 0$, which shall be thought of as the solution of an advection equation using the opposite speed as that for $u(x, t)$, but with *zero* initial data. Then, we get the following 2×2 system:

$$u_t + c u_x = 0, \quad (x, t) \in I \times (0, T], \quad (2.9a)$$

$$\phi_t - c \phi_x = 0, \quad (x, t) \in I \times (0, T], \quad (2.9b)$$

with initial condition $u(x, 0) = u_0(x)$ and $\phi(x, 0) = 0$. Note that this system can be recast into the general form (2.2) with $\mathbf{B}_0 = \text{diag}([c^{-1}, c^{-1}])$, $\mathbf{B}_1 = \begin{bmatrix} 1 & 0 \\ 0 & -1 \end{bmatrix}$.

The semi-discrete DG method for (2.9) is as follows. Find, for any time $t \in (0, T]$, the unique function $(u_h, \phi_h) = (u_h(t), \phi_h(t)) \in V_h^k \times V_h^k$ such that

$$\int_{I_j} (u_h)_t v_h dx - \int_{I_j} c u_h (v_h)_x dx + c^- \widehat{u}_h v_h^-|_{j+\frac{1}{2}} - c^+ \widehat{u}_h v_h^+|_{j-\frac{1}{2}} = 0, \quad (2.10a)$$

$$\int_{I_j} (\phi_h)_t \psi_h dx + \int_{I_j} c \phi_h (\psi_h)_x dx - c^- \widehat{\phi}_h \psi_h^-|_{j+\frac{1}{2}} + c^+ \widehat{\phi}_h \psi_h^+|_{j-\frac{1}{2}} = 0, \quad (2.10b)$$

holds for all $(v_h, \psi_h) \in V_h^k \times V_h^k$ and all $j = 1, \dots, N$. Applying Theorem 2.2, any energy energy conserving numerical fluxes \widehat{u}_h and $\widehat{\phi}_h$ have the following form

$$\widehat{u}_h|_{j-\frac{1}{2}} = \{\!\!\{u_h\}\!\!\} + \alpha_{j-\frac{1}{2}} \llbracket \phi_h \rrbracket, \quad (2.11a)$$

$$\widehat{\phi}_h|_{j-\frac{1}{2}} = \{\!\!\{\phi_h\}\!\!\} + \alpha_{j-\frac{1}{2}} \llbracket u_h \rrbracket. \quad (2.11b)$$

with $\alpha_{j-\frac{1}{2}}$ being any real constant.

We collect this result in the following Corollary.

Corollary 2.4. *The energy*

$$E_h(t) = \int_I (c^{-1}(u_h)^2 + c^{-1}(\phi_h^2)) dx$$

is conserved by the semi-discrete scheme (2.10) with the numerical flux (2.11) for all time.

Remark 2.5 (Modified energy). We specifically remark here that it is the total energy

$$E_h(t) = \int_I (c^{-1}(u_h)^2 + c^{-1}(\phi_h^2)) dx$$

that is conserved, not the quantity $\int_I (c^{-1}(u_h)^2) dx$. The quantity ϕ_h is an approximation to the *zero* function, in general it will not be *zero* as long as $\alpha_{j-\frac{1}{2}} \neq 0$, due to the *coupling* in the numerical flux (2.11).

Now, we turn to the error estimates of the scheme (2.10a). Clearly, taking $\alpha_{j-\frac{1}{2}} = 0$ decouples the two equations (2.10a) and (2.10b), and we obtain the suboptimal DG method with central flux. In the next result, we show that simply taking $\alpha_{j-\frac{1}{2}} = \frac{1}{2}$ for all j results an optimal convergence DG method with a clean proof. The resulting numerical fluxes are

$$\widehat{u}_h|_{j-\frac{1}{2}} = \{\!\!\{u_h\}\!\!\} + \frac{1}{2} \llbracket \phi_h \rrbracket, \quad (2.12a)$$

$$\widehat{\phi}_h|_{j-\frac{1}{2}} = \{\!\!\{\phi_h\}\!\!\} + \frac{1}{2} \llbracket u_h \rrbracket. \quad (2.12b)$$

We start by introducing a set of projections. We shall use the following left and right Gauss-Radau projections P_h^\pm .

$$\int_{I_j} P_h^\pm u(x) v_h dx = \int_{I_j} u(x) v_h dx \quad \forall v_h \in P^{k-1}(I_j), \quad (2.13a)$$

$$(P_h^\pm u)^\pm = u^\pm \quad \text{at } x_{j \mp \frac{1}{2}}, \quad (2.13b)$$

the following approximation properties of P_h^\pm is well-known

$$\|P_h^\pm u - u\|_{I_j} \leq Ch^{k+1}. \quad (2.13c)$$

We shall also use the following coupled projection specifically designed for the DG scheme (2.10). For any function $u, \phi \in H^1(I)$, we introduce the following

coupled auxiliary projection $(P_h^{1,*}u, P_h^{2,*}\phi) \in [V_h^k]^2$:

$$\int_{I_j} P_h^{1,*}u(x)v_h dx = \int_{I_j} u(x)v_h dx \quad \forall v_h \in P^{k-1}(I_j), \quad (2.14a)$$

$$\int_{I_j} P_h^{2,*}\phi(x)v_h dx = \int_{I_j} \phi(x)v_h dx \quad \forall v_h \in P^{k-1}(I_j), \quad (2.14b)$$

$$\left(\{P_h^{1,*}u_h\} + \frac{1}{2} \llbracket P_h^{2,*}\phi_h \rrbracket \right) \Big|_{j-\frac{1}{2}} = u(x_{j-\frac{1}{2}}), \quad (2.14c)$$

$$\left(\{P_h^{2,*}\phi_h\} + \frac{1}{2} \llbracket P_h^{1,*}u_h \rrbracket \right) \Big|_{j-\frac{1}{2}} = \phi(x_{j-\frac{1}{2}}), \quad (2.14d)$$

for all j .

At a first glance, the projection (2.14) seems to be globally coupled. The following Lemma shows that it is actually an optimal local projection.

Lemma 2.6. *The projection (2.14) is well-defined, and it satisfies*

$$P_h^{1,*}u = \frac{1}{2}(P_h^+(u + \phi) + P_h^-(u - \phi)), \quad (2.15a)$$

$$P_h^{2,*}\phi = \frac{1}{2}(P_h^+(u + \phi) - P_h^-(u - \phi)). \quad (2.15b)$$

In particular, it satisfies

$$\|P_h^{1,*}u - u\|_{I_j} \leq Ch^{k+1}, \quad \text{and} \quad \|P_h^{2,*}\phi - \phi\|_{I_j} \leq Ch^{k+1}. \quad (2.15c)$$

Proof. It is clear that the equations (2.14) form a square system, we only need to prove its existence. Adding equations (2.14a) and (2.14b), we get

$$\int_{I_j} (P_h^{1,*}u + P_h^{2,*}\phi)v_h dx = \int_{I_j} (u + \phi)v_h dx, \quad \forall v_h \in P^{k-1}(I_j).$$

Adding equations (2.14c) and (2.14d), we get

$$\underbrace{\left(\{P_h^{1,*}u + P_h^{2,*}\phi\} + \frac{1}{2} \llbracket (P_h^{1,*}u + P_h^{2,*}\phi) \rrbracket \right)}_{=(P_h^{1,*}u + P_h^{2,*}\phi)^+} \Big|_{j-\frac{1}{2}} = u(x_{j-\frac{1}{2}}) + \phi(x_{j-\frac{1}{2}}).$$

This directly implies that $P_h^{1,*}u + P_h^{2,*}\phi = P_h^+(u + \phi)$ by uniqueness of the projection P_h^+ . Similar, we have $P_h^{1,*}u - P_h^{2,*}\phi = P_h^-(u - \phi)$. A simple calculation implies the identities in (2.28). The error estimates are then direct consequences of the estimates in (2.13) for P_h^\pm . \square

Now, we are ready to state our main result on the error estimates.

Theorem 2.7. *Assume that the exact solution u of (2.8) is sufficiently smooth. Let u_h be the numerical solution of the semi-discrete DG scheme (2.10) using the numerical flux (2.12). Then for $T > 0$ there holds the following error estimate*

$$\|u(T) - u_h(T)\|_{L^2(I)} + \|\phi_h(T)\|_{L^2(I)} \leq C(1 + T)h^{k+1}, \quad (2.16)$$

where C is independent of h .

Proof. The proof is a standard energy argument. We only give a sketch. We denote

$$\begin{aligned} \varepsilon_u &:= P_h^{1,*}u - u_h, & \delta_u &:= u - P_h^{1,*}u, \\ \varepsilon_\phi &:= P_h^{2,*}\phi - \phi_h, & \varepsilon_\phi &:= \phi - P_h^{2,*}\phi. \end{aligned} \quad (2.17)$$

Then, consistency the DG scheme 2.10 and definition of the projection (2.14) directly implies that

$$\begin{aligned} \sum_{j=1}^N \left(\int_{I_j} (\varepsilon_u)_t v_h - c \varepsilon_u (v_h)_x dx \right) - (\{\{\varepsilon_u\}\} + \frac{1}{2} \llbracket \varepsilon_\phi \rrbracket) \llbracket c v_h \rrbracket \Big|_{j-\frac{1}{2}} &= \int_I (\delta_u)_t v_h dx, \\ \sum_{j=1}^N \left(\int_{I_j} (\varepsilon_\phi)_t \psi_h + c \varepsilon_\phi (\psi_h)_x dx \right) + (\{\{\varepsilon_\phi\}\} + \frac{1}{2} \llbracket \varepsilon_u \rrbracket) \llbracket c \phi_h \rrbracket \Big|_{j-\frac{1}{2}} &= \int_I (\delta_\phi)_t \phi_h dx, \end{aligned}$$

for all $(v_h, \phi_h) \in [V_h^k]^2$. Taking $v_h = c^{-1} \varepsilon_u$, $\phi_h = c^{-1} \varepsilon_\phi$ (recall that c is a constant on each I_j) in the above error equations and adding, we get the following energy identity

$$\int_I c^{-1} (\varepsilon_u)_t \varepsilon_u + c^{-1} (\varepsilon_\phi)_t \varepsilon_\phi dx = \int_I c^{-1} (\delta_u)_t \varepsilon_u + c^{-1} (\delta_\phi)_t \varepsilon_\phi dx$$

Finally, the error estimate in Theorem 2.7 is obtained by applying the Cauchy-Schwarz inequality, and combing the approximation property of the projection in Lemma 2.6, and an triangle inequality. \square

Remark 2.8 (ϕ_h approximates zero). Note that ϕ_h is an order $k+1$ approximation to the zero function.

Remark 2.9 (A natural extension to systems). This result can be directly used to obtain optimal convergent energy-conserving DG methods for any constant-coefficient, linear symmetric hyperbolic systems (2.2), with a doubling of the unknowns by introducing the auxiliary zero function $\phi(x, t)$ that solves

$$\mathbf{B}_0 \phi_t - \mathbf{B}_1 \phi_x = 0, \quad \forall (x, t) \in I \times (0, T] \quad (2.18)$$

with zero initial condition. The resulting scheme reads as follows: Find, for any time $t \in (0, T]$, the unique functions $(\mathbf{u}_h, \phi_h) \in [V_h^k]^m \times [V_h^k]^m$ such that

$$\left(\int_{I_j} \mathbf{B}_0(\mathbf{u}_h)_t \cdot \mathbf{v}_h - \mathbf{B}_1 \mathbf{u}_h \cdot (\mathbf{v}_h)_x dx \right) + \widehat{\mathbf{B}}_1 \mathbf{u}_h \cdot \mathbf{v}_h^- \Big|_{j+\frac{1}{2}} - \widehat{\mathbf{B}}_1 \mathbf{u}_h \cdot \mathbf{v}_h^+ \Big|_{j-\frac{1}{2}} = 0, \quad (2.19a)$$

$$\left(\int_{I_j} \mathbf{B}_0(\phi_h)_t \cdot \psi_h + \mathbf{B}_1 \phi_h \cdot (\psi_h)_x dx \right) - \widehat{\mathbf{B}}_1 \phi_h \cdot \psi_h^- \Big|_{j+\frac{1}{2}} + \widehat{\mathbf{B}}_1 \phi_h \cdot \psi_h^+ \Big|_{j-\frac{1}{2}} = 0, \quad (2.19b)$$

with the numerical fluxes

$$\widehat{\mathbf{B}}_1 \mathbf{u}_h \Big|_{j-\frac{1}{2}} = \mathbf{B}_1 \{\{\mathbf{u}_h\}\} + \frac{1}{2} \mathbf{B}_1 \llbracket \phi_h \rrbracket, \quad \widehat{\mathbf{B}}_1 \phi_h \Big|_{j-\frac{1}{2}} = \mathbf{B}_1 \{\{\phi_h\}\} + \frac{1}{2} \mathbf{B}_1 \llbracket \mathbf{u}_h \rrbracket. \quad (2.19c)$$

However, doubling the unknowns might be computationally too expensive. For certain special and important cases, e.g. acoustics [28], there exists optimal convergence energy-conserving DG methods without the need of doubling the unknowns. In the next subsection, we derive optimal energy-conserving DG methods for the acoustics equation in a slightly more general form, c.f. [20].

2.4. Optimal energy-conserving DG method for acoustics. In this subsection, we consider the following acoustics equation

$$\begin{bmatrix} p \\ u \end{bmatrix}_t + \begin{bmatrix} u_0 & K_0 \\ 1/\rho_0 & u_0 \end{bmatrix} \begin{bmatrix} p \\ u \end{bmatrix}_x = 0, \quad (x, t) \in I \times (0, T]. \quad (2.20)$$

with a smooth periodic initial condition and a periodic boundary condition. Here u is the velocity, p is the pressure, and u_0 is the background velocity, ρ_0 is the background density, and K_0 is the *bulk modulus of compressibility* of the material, c.f. [20]. The coefficients ρ_0, u_0 and K_0 are assumed to be positive constants.

Note that the equation (2.20) is a 2×2 linear symmetric hyperbolic system, which can be recast into the form (2.2) with $\mathbf{u} = [p, u]'$, and the coefficient matrices

$$\mathbf{B}_0 = \begin{bmatrix} 1/K_0 & 0 \\ 0 & \rho_0 \end{bmatrix}, \quad \text{and} \quad \mathbf{B}_1 = \begin{bmatrix} u_0/K_0 & 1 \\ 1 & u_0\rho_0 \end{bmatrix}. \quad (2.21)$$

We see that the energy

$$E(t) = \int_I (p(x)^2/K_0 + \rho_0 u(x)^2) dx \quad (2.22)$$

is conserved for the system (2.20).

Theorem 2.2 implies that semi-discrete energy-conserving DG method for the resulting 2×2 symmetric hyperbolic system shall be of the form (2.3) with the coefficient matrices (2.21), and the following numerical flux

$$\widehat{\mathbf{B}}_1 \mathbf{u}_h|_{j-\frac{1}{2}} = \mathbf{B}_1 \{\{\mathbf{u}_h\}\} + \alpha_{j-\frac{1}{2}} \begin{bmatrix} 0 & 1 \\ -1 & 0 \end{bmatrix} \llbracket \mathbf{u}_h \rrbracket, \quad (2.23)$$

with $\alpha_{j-1/2}$ a scalar constant for all j .

Translating this condition back to the non-symmetric system (2.20), we get the following equivalent formulation of the method. Find, for any time $t \in (0, T]$, the unique function $(p_h, u_h) = (p_h(t), u_h(t)) \in V_h^k \times V_h^k$ such that

$$\int_{I_j} (p_h)_t q_h - (u_0 p_h + K_0 u_h)(q_h)_x dx + \widehat{f}_h q_h^-|_{j+\frac{1}{2}} - \widehat{f}_h q_h^+|_{j-\frac{1}{2}} = 0, \quad (2.24a)$$

$$\int_{I_j} (u_h)_t v_h - (p_h/\rho_0 + u_0 u_h)(v_h)_x dx + \widehat{g}_h q_h^-|_{j+\frac{1}{2}} - \widehat{g}_h q_h^+|_{j-\frac{1}{2}} = 0, \quad (2.24b)$$

for all $(q_h, v_h) \in V_h^k \times V_h^k$, for all j , where the numerical fluxes \widehat{f}_h and \widehat{g}_h are given by

$$\widehat{f}_h = u_0 \{\{p_h\}\} + K_0 \{\{u_h\}\} + \alpha_{j-\frac{1}{2}} K_0 \llbracket u_h \rrbracket, \quad (2.24c)$$

$$\widehat{g}_h = \{\{p_h\}\}/\rho_0 + u_0 \{\{u_h\}\} - \alpha_{j-\frac{1}{2}} \llbracket p_h \rrbracket/\rho_0. \quad (2.24d)$$

We state the energy-conservation property of this method in the following Corollary.

Corollary 2.10. *The energy*

$$E_h(t) = \int_I (p_h(x)^2/K_0 + \rho_0 u_h(x)^2) dx$$

is conserved by the semi-discrete scheme (2.24) for all time.

Remark 2.11 (Alternating flux). In the special case when $u_0 = 0$, taking $\alpha_{j-\frac{1}{2}} = 1/2$ for all j , or $\alpha_{j-\frac{1}{2}} = -1/2$ for all j , results the optimal convergent, energy conserving DG method with an alternating flux considered in [28].

Next, we turn to the error estimates of the scheme (2.24) with a proper choice of the *stabilization* parameter $\alpha_{j-\frac{1}{2}}$. It turns out the error estimates is drastically different, which depends on whether the background velocity u_0 is subsonic ($u_0 < c_0$) or supersonic ($u_0 > c_0$), where $c_0 := \sqrt{K_0/\rho_0}$ is the speed of sound.

2.4.1. *Subsonic case* ($u_0 < c_0$). In this case, the matrix \mathbf{B}_1 has a positive eigenvalue and a negative eigenvalue. In particular, there exists an orthogonal matrix \mathbf{S} with determinant 1 such that

$$\mathbf{B}_1 = \mathbf{S} \operatorname{diag}([\lambda_+, \lambda_-]) \mathbf{S}^{-1}, \quad (2.25)$$

with $\lambda_+ > 0 > \lambda_-$ being the two roots of the quadratic equation

$$(\lambda - u_0/K_0)(\lambda - u_0\rho_0) - 1 = 0.$$

We have $\lambda_- \lambda_+ = \frac{u_0^2}{c_0^2} - 1 < 0$. A simple calculation yields that, for any orthogonal matrix $\mathbf{S} \in \mathbb{R}^{2 \times 2}$ with determinant 1, there holds

$$\mathbf{S} \begin{bmatrix} 0 & 1 \\ -1 & 0 \end{bmatrix} \mathbf{S}^{-1} = \begin{bmatrix} 0 & 1 \\ -1 & 0 \end{bmatrix}, \quad (2.26)$$

which will be used in the proof of Lemma 2.12 below.

We take the stabilization parameter $\alpha_{j-\frac{1}{2}} = \frac{1}{2} \sqrt{-\lambda_- \lambda_+} = \frac{1}{2} \sqrt{1 - \frac{u_0^2}{c_0^2}}$.

To derive the optimal error estimate, we shall use the following coupled projection. We work with vector notation. For any function $\mathbf{u} = (u_1, u_2) \in [H^1(I)]^2$, we introduce the following coupled auxiliary projection $P_h^* \mathbf{u} \in [V_h^k]^2$:

$$\int_{I_j} P_h^* \mathbf{u} \cdot \mathbf{v}_h \, dx = \int_{I_j} \mathbf{u}(x) \cdot \mathbf{v}_h \, dx \quad \forall \mathbf{v}_h \in [P^{k-1}(I_j)]^2, \quad (2.27a)$$

$$(\mathbf{B}_1 \{P_h^* \mathbf{u}_h\}) + \alpha \begin{bmatrix} 0 & 1 \\ -1 & 0 \end{bmatrix} \llbracket P_h^* \mathbf{u}_h \rrbracket \Big|_{j-\frac{1}{2}} = \mathbf{B}_1 \mathbf{u}(x_{j-\frac{1}{2}}), \quad (2.27b)$$

for all j , where $\alpha = \frac{1}{2} \sqrt{1 - \frac{u_0^2}{c_0^2}}$ is the stabilization parameter.

Similar to the advection case in Lemma 2.6, the above projection is also an optimal local projection.

Lemma 2.12. *The projection (2.27) is well-defined, and it satisfies*

$$P_h^* \mathbf{u} = \mathbf{S} \begin{bmatrix} \Pi_h^{1,*} w_1 \\ \Pi_h^{2,*} w_2 \end{bmatrix}, \quad (2.28a)$$

where $\mathbf{w} = (w_1, w_2) = \mathbf{S}^{-1} \mathbf{u}$ is the characteristic variable, and

$$\Pi_h^{1,*} w_1 = \frac{1}{2} P_h^+ \left(w_1 + \sqrt{\frac{\lambda_+}{-\lambda_-}} w_2 \right) + \frac{1}{2} P_h^- \left(w_1 - \sqrt{\frac{\lambda_+}{-\lambda_-}} w_2 \right), \quad (2.28b)$$

$$\Pi_h^{2,*} w_2 = \frac{1}{2} P_h^+ \left(w_2 + \sqrt{\frac{-\lambda_-}{\lambda_+}} w_1 \right) + \frac{1}{2} P_h^- \left(w_2 - \sqrt{\frac{-\lambda_-}{\lambda_+}} w_1 \right), \quad (2.28c)$$

In particular, it satisfies

$$\|P_h^* \mathbf{u} - \mathbf{u}\|_{I_j} \leq Ch^{k+1}. \quad (2.28d)$$

Proof. The proof follows the lines for that for Lemma 2.6. We first turn to projection for the characteristic variable \mathbf{w} , and then transform back to the primitive variable \mathbf{u} . Since \mathbf{B}_1 and \mathbf{S} are constant matrices, we have $\mathbf{S}^{-1}P_h^*\mathbf{u} = P_h^*(\mathbf{S}^{-1}\mathbf{u}) = P_h^*\mathbf{w}$. Multiplying both sides of equation (2.27a) by \mathbf{S} , and both side of equations (2.27b) by $\Lambda^{-1}\mathbf{S}^{-1}$, and using the fact that $\alpha = \frac{1}{2}\sqrt{-\lambda_- \lambda_+}$ and using the equation (2.26), we get the following projection for the characteristic variable \mathbf{w} :

$$\int_{I_j} P_h^* \mathbf{w} \cdot \mathbf{v}_h dx = \int_{I_j} \mathbf{w}(x) \cdot \mathbf{v}_h dx \quad \forall \mathbf{v}_h \in [P^{k-1}(I_j)]^2,$$

$$\left(\llbracket P_h^* \mathbf{w} \rrbracket + \frac{1}{2} \begin{bmatrix} 0 & \sqrt{-\lambda_- / \lambda_+} \\ \sqrt{-\lambda_+ / \lambda_-} & 0 \end{bmatrix} \llbracket P_h^* \mathbf{w}_h \rrbracket \right) \Big|_{j-\frac{1}{2}} = \mathbf{w}(x_{j-\frac{1}{2}}).$$

A similar algebraic manipulation as that in the proof of Lemma 2.6 yields

$$\sqrt{\lambda_+} P_h^{1,*} w_1 \pm \sqrt{\lambda_-} P_h^{1,*} w_2 = P_h^\pm (\sqrt{\lambda_+} w_1 + \sqrt{-\lambda_-} w_2),$$

and the equalities and estimate (2.28) in Lemma 2.12 follow directly. \square

With the help of this projection, optimal error estimates follow directly. We skip the proof, which is identical to the proof of Theorem 2.7.

Theorem 2.13. *Assume that the exact solution (p, u) of (2.20) is sufficiently smooth. Let (p_h, u_h) be the numerical solution of the semi-discrete DG scheme (2.24) with $\alpha_{j-\frac{1}{2}} = \sqrt{1 - u_0^2/c_0^2}$ in the numerical fluxes (2.24c) and (2.24d). Then for $T > 0$ there holds the following error estimate*

$$\|u(T) - u_h(T)\|_{L^2(I)} + \|p(T) - p_h(T)\|_{L^2(I)} \leq C(1+T)h^{k+1}, \quad (2.29)$$

where C is independent of h .

2.4.2. Supersonic case ($u_0 > c_0$). In this case, the eigenvalues of the matrix \mathbf{B}_1 are all positive, the construction of a local projection P_h^* in the previous section is no longer valid. Hence, we suggest the doubling the unknowns approach, c.f. Remark 2.9, to obtain an optimal convergent, energy-conserving semi-discrete DG scheme on general nonuniform meshes.

However, if we insist in working with the original system and use scheme (2.24), we can take the stabilization parameter $\alpha = \frac{1}{2}\sqrt{\frac{u_0^2}{c_0^2} - 1}$. The resulting method can be proven to be optimally convergent on *uniform* meshes for all polynomial degree, but only suboptimal convergent on *nonuniform* meshes. The optimal convergence of this method for all polynomial degree is numerically verified, and a loss of convergence order is also numerically observed on nonuniform randomly perturbed meshes. These numerical tests are not reported in the paper to save space.

The corresponding error analysis is also more involved, which follows from similar arguments as in [2, 4]. Without further going into details, we claim that we can prove the projection (2.27) is a well-defined *global* projection for all polynomial degree $k \geq 0$, in the supersonic case ($u_0 > c_0$), which has the approximation property $\|P_h^* \mathbf{u} - \mathbf{u}\|_{L^2(I)} \leq Ch^{\tilde{k}}$, where $\tilde{k} = k + 1$ on uniform meshes, and $\tilde{k} = k$ on general nonuniform meshes. We specifically remark that the global projections defined in [2, 4] require the polynomial degree to be even, otherwise is not well-defined. But due to the coupling term (2.27b), we do not have this polynomial degree restriction for well-possesses of the projection (2.27). In particular, we do obtain optimal convergence on uniform meshes for *any* polynomial degree.

2.5. Optimal energy-conserving DG methods for linear symmetric hyperbolic systems. Now, we turn back to the general, m -component, linear symmetric hyperbolic systems (2.2) with a diagonal, piecewise constant, positive matrix $\mathbf{B}_0 \in \mathbb{R}^{m \times m}$, and a symmetric constant matrix $\mathbf{B}_1 \in \mathbb{R}^{m \times m}$.

We shall consider the eigenvalue decomposition of \mathbf{B}_1 . Without loss of generality, we assume that the number of positive eigenvalues for \mathbf{B}_1 is always greater than or equal to the number of its negative eigenvalues. Hence, we assume that \mathbf{B}_1 has $r + s$ positive eigenvalues $\{\lambda_i^+\}_{i=1}^{r+s}$, and s negative eigenvalues, $\{\lambda_{r+s+1-i}^-\}_{i=1}^s$, with non-negative integers r and s satisfying $r + 2s \leq m$. These *nonzero* eigenvalues are ordered such that

$$\lambda_1^+ \geq \lambda_2^+ \geq \cdots \lambda_{r+s}^+ > 0 > \lambda_{r+s}^- \geq \cdots \geq \lambda_{r+1}^-.$$

We denote the diagonal eigenvalue matrix of \mathbf{B}_1 as

$$\Lambda = \text{diag}([\lambda_1^+, \cdots, \lambda_{r+s}^+, \underbrace{0, \cdots, 0}_{m-r-2s \text{ zeros}}, \lambda_{r+s}^-, \cdots, \lambda_{r+1}^-]) \in \mathbb{R}^{m \times m}, \quad (2.30a)$$

and the corresponds orthogonal eigenvalue decomposition

$$\mathbf{B}_1 = \mathbf{S} \Lambda \mathbf{S}^{-1}, \quad \mathbf{S} \in \mathbb{R}^{m \times m} \text{ is orthogonal with determinant 1.} \quad (2.30b)$$

We denote the characteristic variable $\mathbf{w} = (w_1, \cdots, w_m) = \mathbf{S}^{-1} \mathbf{u}$, so the characteristic component w_i has wave speed $\Lambda(i, i)$.

Based on the discussion in the previous two subsection, for each positive integer $\mu \leq s$, we shall pair the characteristic variables $w_{r+\mu}$, with wave speed $\lambda_{r+\mu}^+$, and $w_{m+1-\mu}$, with wave speed $\lambda_{r+\mu}^-$, and consider the optimal energy-conserving numerical flux (2.23) for the pair $(w_{r+\mu}, w_{m+1-\mu})$. And for the remaining r variables, we shall follow the discussion in subsection 2.3 to introduce auxiliary *zero* variables that travel with the negative speed $\lambda_\mu^- := -\lambda_\mu^+$ for $1 \leq \mu \leq r$. To be more precise, we consider the following $m + r$ component, augmented system for the variable $\tilde{\mathbf{u}} = [\mathbf{u}; \boldsymbol{\phi}]$:

$$\widetilde{\mathbf{B}}_0 \tilde{\mathbf{u}}_t + \widetilde{\mathbf{B}}_1 \tilde{\mathbf{u}}_x = 0, \quad (x, t) \in I \times (0, T], \quad (2.31a)$$

with

$$\widetilde{\mathbf{B}}_0 = \begin{bmatrix} \mathbf{B}_0 & 0 \\ 0 & \mathbf{I}_r \end{bmatrix}, \quad \text{and} \quad \widetilde{\mathbf{B}}_1 = \begin{bmatrix} \mathbf{B}_1 & 0 \\ 0 & \text{diag}([\lambda_r^-, \cdots, \lambda_1^-]) \end{bmatrix}, \quad (2.31b)$$

with initial condition $\tilde{\mathbf{u}}(x, 0) = [\mathbf{u}(x); 0]$. Here \mathbf{I}_r is the $r \times r$ identity matrix and $\boldsymbol{\phi}$ has r components. Note that the augmented matrix $\widetilde{\mathbf{B}}_1$ has the following eigenvalue decomposition

$$\widetilde{\mathbf{B}}_1 = \widetilde{\mathbf{S}} \widetilde{\Lambda} \widetilde{\mathbf{S}}^{-1}, \quad (2.32a)$$

with

$$\widetilde{\Lambda} = \text{diag}([\lambda_1^+, \cdots, \lambda_{r+s}^+, \underbrace{0, \cdots, 0}_{m-r-2s \text{ zeros}}, \lambda_{r+s}^-, \cdots, \lambda_1^-]), \quad (2.32b)$$

and

$$\widetilde{\mathbf{S}} = \begin{bmatrix} \mathbf{S} & 0 \\ 0 & \mathbf{I}_r \end{bmatrix}. \quad (2.32c)$$

To further simplify notation, for each positive integer $\mu \leq r + s$ we denote the anti-symmetric $(m + r) \times (m + r)$ matrices $\widetilde{\mathbf{R}}_\mu$ that only has non-vanishing components on the $(\mu, m + r - \mu)$ and $(m + r - \mu, \mu)$ locations, with

$$\widetilde{\mathbf{R}}_\mu(\mu, m + r - \mu) = 1, \quad \text{and} \quad \widetilde{\mathbf{R}}_\mu(m + r - \mu, \mu) = -1.$$

Finally, we are ready to state our main result on the optimal energy conserving semi-discrete DG method for the augmented system (2.31). The proof is omitted since it directly follows from the discussion in the previous two subsection.

Theorem 2.14. *Assume that the exact solution $\widetilde{\mathbf{u}}$ of (2.31) is sufficiently smooth. Let $\widetilde{\mathbf{u}}_h \in [V_h^k]^{m+r}$ be the numerical solution of the following semi-discrete DG scheme:*

$$\begin{aligned} \int_{I_j} \widetilde{\mathbf{B}}_0(\widetilde{\mathbf{u}}_h)_t \cdot \widetilde{\mathbf{v}}_h dx - \int_{I_j} \widetilde{\mathbf{B}}_1 \widetilde{\mathbf{u}}_h \cdot (\widetilde{\mathbf{v}}_h)_x dx \\ + \widehat{\widetilde{\mathbf{B}}_1 \widetilde{\mathbf{u}}_h} \cdot \widetilde{\mathbf{v}}_h^-|_{j+\frac{1}{2}} - \widehat{\widetilde{\mathbf{B}}_1 \widetilde{\mathbf{u}}_h} \cdot \widetilde{\mathbf{v}}_h^+|_{j-\frac{1}{2}} = 0, \end{aligned} \quad (2.33a)$$

for all $\widetilde{\mathbf{v}}_h \in [V_h^k]^{m+r}$ and all $j = 1, \dots, N$, with the numerical flux

$$\widehat{\widetilde{\mathbf{B}}_1 \widetilde{\mathbf{u}}_h}|_{j-\frac{1}{2}} = \widetilde{\mathbf{B}}_1 \{\{\widetilde{\mathbf{u}}_h\}\} + \frac{1}{2} \sum_{\mu=1}^{r+s} \sqrt{|\lambda_\mu^+ \lambda_\mu^-|} \widetilde{\mathbf{S}} \widetilde{\mathbf{R}}_\mu \widetilde{\mathbf{S}}^{-1} \llbracket \widetilde{\mathbf{u}}_h \rrbracket, \quad (2.33b)$$

Then, the total energy

$$\widetilde{E}(t) = \int_I (\widetilde{\mathbf{B}}_0 \widetilde{\mathbf{u}}_h) \cdot \widetilde{\mathbf{u}}_h dx$$

is conserved for all time. Moreover, for $T > 0$ there holds the following error estimate

$$\|\widetilde{\mathbf{u}}(T) - \widetilde{\mathbf{u}}_h(T)\|_{L^2(I)} \leq C(1 + T)h^{k+1}, \quad (2.34)$$

where C is independent of h .

Remark 2.15 (Doubling the unknowns). If we simply double the unknowns, the scheme (2.33) applied to the resulting coupled system (2.2) and (2.18) is slightly different from the scheme (2.19) introduced in Remark 2.9, with the only difference being the numerical flux (2.19c) replaced by the following characteristic-wise one:

$$\widehat{\mathbf{B}}_1 \mathbf{u}_h|_{j-\frac{1}{2}} = \mathbf{B}_1 \{\{\mathbf{u}_h\}\} + \frac{1}{2} |\mathbf{B}_1| \llbracket \phi_h \rrbracket, \quad \widehat{\mathbf{B}}_1 \phi_h|_{j-\frac{1}{2}} = \mathbf{B}_1 \{\{\phi_h\}\} + \frac{1}{2} |\mathbf{B}_1| \llbracket \mathbf{u}_h \rrbracket, \quad (2.35)$$

where $|\mathbf{B}_1| = \mathbf{S} |\boldsymbol{\Lambda}| \mathbf{S}^{-1}$. Although this flux is slightly more expensive than the component-wise flux (2.19c) with both methods optimally convergent, the extension of the flux (2.35) to multi-dimensions on unstructured meshes is more promising than that for (2.19c). See also Remark 3.3 below.

2.6. High-order energy-conserving Lax-Wendroff time discretization. In this section, we consider the temporal discretization of the semi-discrete scheme (2.33). We introduce an explicit, high-order, energy-conserving Lax-Wendroff time integrator.

To simplify notation, we denote

$$M_h(\tilde{\mathbf{u}}_h, \tilde{\mathbf{v}}_h) := \sum_{j=1}^N \int_{I_j} \widetilde{\mathbf{B}}_0 \tilde{\mathbf{u}}_h \cdot \tilde{\mathbf{v}}_h dx \quad (2.36a)$$

$$B_h(\tilde{\mathbf{u}}_h, \tilde{\mathbf{v}}_h) := \sum_{j=1}^N \left(\int_{I_j} \widetilde{\mathbf{B}}_1 \tilde{\mathbf{u}}_h \cdot (\tilde{\mathbf{v}}_h)_x dx + \widetilde{\mathbf{B}}_1 \tilde{\mathbf{u}}_h \cdot [\tilde{\mathbf{v}}_h] \Big|_{j-\frac{1}{2}} \right). \quad (2.36b)$$

The semi-discrete scheme (2.33) is to find $\tilde{\mathbf{u}}_h(t) \in [V_h^k]^{m+d}$ such that

$$M_h((\tilde{\mathbf{u}}_h)_t, \tilde{\mathbf{v}}_h) = B_h(\tilde{\mathbf{u}}_h, \tilde{\mathbf{v}}_h), \quad \forall \tilde{\mathbf{v}}_h \in [V_h^k]^{m+d}. \quad (2.37)$$

Introducing a set of basis, e.g. orthogonal Legendre polynomials, for the DG space V_h^k , and denoting $[\mathbf{u}_h(t)]$ as the vector of degrees of freedom for $\tilde{\mathbf{u}}_h(t)$, the above semi-discrete scheme can be expressed as the following matrix-vector form:

$$[\mathbf{u}_h]_t = \mathbf{M}^{-1} \mathbf{A}[\mathbf{u}_h], \quad (2.38)$$

where \mathbf{M} is the ($\widetilde{\mathbf{B}}_0$ -weighted) mass matrix, which is diagonal if one choose the Legendre basis, and \mathbf{A} is the matrix corresponding to the spatial operator $B_h(\cdot, \cdot)$. A reformulation of the energy conservation property of the scheme (2.33) in Theorem 2.14 in this matrix-vector notation is given below:

$$(\mathbf{M}[\mathbf{u}_h(t)]) \cdot [\mathbf{u}_h(t)] = (\mathbf{M}[\mathbf{u}_h(0)]) \cdot [\mathbf{u}_h(0)], \quad \forall t > 0, \quad (2.39a)$$

$$\mathbf{A} \text{ is anti-symmetric.} \quad (2.39b)$$

Now, we consider a class of Lax-Wendroff time discretization for the semi-discrete scheme (2.38) that preserve a discrete version of the energy conservation identity (2.39a). The Lax-Wendroff time discretization [19] is a high-order method known as the Cauchy-Kowalewski type procedure in the literature, which relies on converting each time derivative in a truncated temporal Taylor expansion (with expected accuracy) of the solution into spatial derivatives by repeatedly using the underlying differential equation and its differentiated form. We directly work with the semi-discrete scheme (2.38) without going back to the PDE (2.31).

Let $0 = t_0 < t_1 < \dots < t_N = T$ be a partition of the interval $[0, T]$ with time step $\Delta t = t_{n+1} - t_n$. Here uniform time step Δt is used. For, any non-negative integer r , a temporal $(2r + 1)$ -th stage, $(2r + 2)$ -th order accurate fully discrete approximation $[\mathbf{u}_h^n]$ for (2.38) are construction as follows: for $n = 1, \dots, N - 1$, $[\mathbf{u}_h^{n+1}]$ is given by

$$[\mathbf{u}_h^{n+1}] - [\mathbf{u}_h^{n-1}] = \sum_{i=0}^r \frac{2\Delta t^{2i+1}}{(2i+1)!} (\mathbf{M}^{-1} \mathbf{A})^{2i+1} [\mathbf{u}_h^n]. \quad (2.40)$$

We specifically mention that the above time discretization is obtained by the following Taylor approximation and the Lax-Wendroff procedure of converting the time derivatives into the discrete spatial operators using (2.38),

$$u(t + \Delta t) - u(t - \Delta t) = \sum_{i=0}^r \frac{2\Delta t^{2i+1}}{(2i+1)!} u^{(2i+1)}(t) + \mathcal{O}(\Delta t^{2r+2}).$$

Note that for $r = 0$, we get the usual second-order accurate leap-frog method

$$[\mathbf{u}_h^{n+1}] - [\mathbf{u}_h^{n-1}] = 2\Delta t \mathbf{M}^{-1} \mathbf{A}[\mathbf{u}_h^n].$$

The energy conservation property of the fully discrete scheme is documented in the next theorem.

Theorem 2.16. *The fully discrete scheme (2.40) satisfies the energy identity*

$$(\mathbf{M}[\mathbf{u}_h^{n+1}]) \cdot [\mathbf{u}_h^n] = (\mathbf{M}[\mathbf{u}_h^n]) \cdot [\mathbf{u}_h^{n-1}]$$

Proof. The equality is obtained by dotting the equation (2.40) with $\mathbf{M}[\mathbf{u}_h^n]$, and taking into account the anti-symmetry of the matrix \mathbf{A} , (2.39b). \square

Remark 2.17 (Runge-Kutta type time discretization). Recall that the r -stage r -th order accurate explicit Runge-Kutta method for (2.38) can be write as the following Lax-Wendroff form, cf. [26],

$$[\mathbf{u}_h^{n+1}] - [\mathbf{u}_h^n] = \sum_{i=1}^r \frac{\Delta t^i}{(i)!} (\mathbf{M}^{-1} \mathbf{A})^i [\mathbf{u}_h^n]. \quad (2.41)$$

This time discretization is not energy-conserving.

Remark 2.18 (Time-dependent source term). The above time discretization (2.40) and (2.41) can be easily modified to treat a *linear* time-dependent source term without sacrificing its formal order of accuracy. In particular, consider the follow system of ODEs:

$$[\mathbf{u}_h]_t = \mathbf{M}^{-1} \left(\mathbf{A}[\mathbf{u}_h] + [\mathbf{f}(t)] \right), \quad (2.42)$$

with $\mathbf{f}(t)$ takes into account possible *linear* boundary/volume source terms. The energy-conserving Lax-Wendroff method then reads

$$[\mathbf{u}_h^{n+1}] - [\mathbf{u}_h^{n-1}] = \sum_{i=0}^r \left(\frac{2\Delta t^{2i+1}}{(2i+1)!} [d^{2i+1} \mathbf{u}_h^n] \right), \quad (2.43a)$$

where $[d^0 \mathbf{u}_h] = [\mathbf{u}_h]$, and $[d^s \mathbf{u}_h]$, $s \geq 1$, is recursively defined through the following map:

$$[d^s \mathbf{u}_h^n] = \mathbf{M}^{-1} \left(\mathbf{A} [d^{s-1} \mathbf{u}_h^n] + [\mathbf{f}^{(s-1)}(t)] \right) \quad s \geq 1, \quad (2.43b)$$

with $\mathbf{f}^{(s-1)}(t)$ being the $(s-1)$ -th derivative of $\mathbf{f}(t)$. And the Runge-Kutta type Lax-Wendroff method reads

$$[\mathbf{u}_h^{n+1}] - [\mathbf{u}_h^n] = \sum_{i=0}^r \left(\frac{\Delta t^{i+1}}{(i+1)!} [d^{i+1} \mathbf{u}_h^n] \right), \quad (2.43c)$$

We specifically mention the Lax-Wendroff method (2.43c) is different from the classical Runge-Kutta method for the time-dependent source term treatment. The Runge-Kutta method is well-known to suffer from the so-called order reduction when boundary source term were not properly adjusted, c.f. [3]. But the Lax-Wendroff methods (2.43a) and (2.43c) do not suffer from such order reduction since all spatial derivatives are calculated on the same time level.

Remark 2.19 (Lax-Wendroff time discretization for nonlinear equations). We shall point out that the Lax-Wendroff method is considerably more complex to derive for nonlinear equations; see [14, 19], as one would need to take into account the time derivative of the matrix \mathbf{A} , that depends on the solution \mathbf{u}_h . In this case, instead of the current method of lines approach (first spatial DG discretization, then temporal Lax-Wendroff discretization), we shall first discretize the PDE in time then apply a proper spatial DG discretization, which takes into account higher order derivatives.

2.7. Boundary treatment. For boundary value problems, special care need to be taken for the numerical fluxes at the boundary. Here we discuss how to impose the inflow boundary conditions.

Consider the linear symmetric hyperbolic system (2.31), where we suppressed the tilde notation for ease of presentation, with initial condition $\mathbf{u}(x, 0) = \mathbf{u}_0$, and *inflow* boundary condition

$$\mathbf{B}_1^+ \mathbf{u}(a, t) = \mathbf{B}_1^+ \mathbf{u}_a(t), \quad \mathbf{B}_1^- \mathbf{u}(b, t) = \mathbf{B}_1^- \mathbf{u}_b(t), \quad (2.44a)$$

where

$$\mathbf{B}_1^+ = \mathbf{S} \operatorname{diag}([\max(\lambda_1, 0), \dots, \max(\lambda_{m+r}, 0)]) \mathbf{S}^{-1}, \quad (2.44b)$$

$$\mathbf{B}_1^- = \mathbf{S} \operatorname{diag}([\min(\lambda_1, 0), \dots, \min(\lambda_{m+r}, 0)]) \mathbf{S}^{-1}, \quad (2.44c)$$

and $\mathbf{B}_1 = \mathbf{S} \operatorname{diag}([\lambda_1, \dots, \lambda_{m+r}]) \mathbf{S}^{-1}$ is an eigenvalue decomposition of \mathbf{B}_1 . We denote $|\mathbf{B}_1| := \mathbf{B}_1^+ - \mathbf{B}_1^-$. We further assume that all eigenvalues of \mathbf{B}_1 are non-zero. The PDE (2.31) (ignoring the tilde notation) with the boundary condition has the following energy identity:

$$\begin{aligned} \frac{d}{dt} \left(\frac{1}{2} \int_I \mathbf{B}_0 \mathbf{u}(t) \cdot \mathbf{u}(t) dx \right) - \frac{1}{2} \mathbf{B}_1^- \mathbf{u}(a, t) \cdot \mathbf{u}(a, t)^2 + \frac{1}{2} \mathbf{B}_1^+ \mathbf{u}(b, t) \cdot \mathbf{u}(b, t)^2 \\ = \frac{1}{2} \mathbf{B}_1^+ \mathbf{u}_a(t) \cdot \mathbf{u}_a(t) - \frac{1}{2} \mathbf{B}_1^- \mathbf{u}_b(t) \cdot \mathbf{u}_b(t). \end{aligned} \quad (2.45)$$

On the two end points of the interval I , we simply take the following upwinding numerical flux:

$$\widehat{\mathbf{B}_1 \mathbf{u}_h}|_{x=a} = \mathbf{B}_1^+ \mathbf{u}_a + \mathbf{B}_1^- \mathbf{u}_h^+|_{x=a}, \quad (2.46a)$$

$$\widehat{\mathbf{B}_1 \mathbf{u}_h}|_{x=b} = \mathbf{B}_1^- \mathbf{u}_b + \mathbf{B}_1^+ \mathbf{u}_h^+|_{x=b}. \quad (2.46b)$$

The resulting semi-discrete scheme enjoys a similar energy identity as (2.45) and is optimal convergent. The proof is similar to the periodic case (2.14), and is omitted for simplicity.

Theorem 2.20. *Assume that the exact solution $\tilde{\mathbf{u}}$ of (2.31) with boundary condition (2.44a) is sufficiently smooth. Let $\tilde{\mathbf{u}}_h \in [V_h^k]^{m+r}$ be the numerical solution of (2.33) with internal (energy-conserving) numerical flux (2.33b), and boundary (upwinding) numerical flux (2.46). Then, the following energy identity holds*

$$\begin{aligned} \frac{d}{dt} \left(\frac{1}{2} \int_I \mathbf{B}_0 \mathbf{u}_h(t) \cdot \mathbf{u}_h(t) dx \right) + \frac{1}{2} |\mathbf{B}_1| \mathbf{u}_h^+ \cdot \mathbf{u}_h^+ \Big|_{x=a} + \frac{1}{2} |\mathbf{B}_1| \mathbf{u}_h^- \cdot \mathbf{u}_h^- \Big|_{x=b} \\ = \mathbf{B}_1^- \mathbf{u}_a(t) \cdot \mathbf{u}_h^+|_{x=a} - \mathbf{B}_1^- \mathbf{u}_b(t) \cdot \mathbf{u}_h^-|_{x=b}. \end{aligned} \quad (2.47)$$

Moreover, for $T > 0$ there holds the following error estimate

$$\|\mathbf{u}(T) - \mathbf{u}_h(T)\|_{L^2(I)} \leq C(1+T)h^{k+1}, \quad (2.48)$$

where C is independent of h .

Remark 2.21 (Time discretization, stability issue). The semi-discrete DG scheme for the boundary value problem naturally leads to the ODE system (2.42), where $\mathbf{f}(t)$ takes into account the boundary condition. We can simply apply the time-discretization (2.43a) or (2.43c) as discussed in Remark 2.18.

However, our numerical results, not reported in this paper, showed that the resulting fully discrete scheme using the time discretization (2.43a) is *unconditionally unstable*. Such instability was not observed for the Runge-Kutta type time discretization (2.43c).

Similar boundary-driven instability was documented in the literature for energy-conserving schemes such as the finite difference leap-frog method, c.f. [1], which is identical to the lowest-order P^0 -DG method with a central flux and a leap-frog time stepping on uniform meshes. One remedy to cure this instability for the leap-frog method, c.f. [1], was to simply modify the leap-frog time-stepping on cells that touch the boundary to be a forward Euler time stepping.

We can extend this idea to the higher-order Lax-Wendroff methods as follows: for cells not touching the boundary, use the $(2r + 1)$ -stage energy-conserving Lax-Wendroff method (2.43a), and for cells that touch the boundary, use the $(2r + 1)$ -stage Runge-Kutta type Lax-Wendroff method (2.43c). The resulting scheme is numerically shown, with results not reported in this paper to save space, to be high-order accurate and conditionally stable, although a detailed stability analysis is missing.

3. ENERGY-CONSERVING DG METHODS FOR THE MULTIDIMENSIONAL CASE

In this section, we present the energy-conserving DG methods for the multi-dimensional symmetric linear hyperbolic systems. Without loss of generality, we describe our DG scheme in two dimensions ($d = 2$); all the arguments can be easily extended to the more general cases $d > 2$.

We shall restrict ourselves mainly to the following two-dimensional system of linear symmetric hyperbolic conservation laws problem

$$\mathbf{B}_0 \mathbf{u}_t + \mathbf{B}_1 \mathbf{u}_x + \mathbf{B}_2 \mathbf{u}_y = 0, \quad (x, y, t) \in \Omega \times (0, T], \quad (3.1a)$$

$$\mathbf{u}(x, y, 0) = \mathbf{u}_0(x, y), \quad (x, y) \in \Omega, \quad (3.1b)$$

where $\mathbf{B}_0 : \Omega \rightarrow \mathbb{R}^{m \times m}$ is a positive, piecewise-constant, diagonal matrix, $\mathbf{B}_1, \mathbf{B}_2 \in \mathbb{R}^{m \times m}$ are two symmetric matrices. For the sake of simplicity, we consider only the periodic boundary conditions.

Given any direction field $\mathbf{n} = (n_x, n_y)$, we denote the matrix

$$\mathbf{B}_{\mathbf{n}} := n_x \mathbf{B}_1 + n_y \mathbf{B}_2. \quad (3.2)$$

Based on the one-dimensional results, we shall first derive an energy-conserving DG methods for (3.1) in the case when the matrix $\mathbf{B}_{\mathbf{n}}$ has the same number of positive and negative eigenvalues for any direction \mathbf{n} , denoted as $r_{\mathbf{n}} \geq 0$. The number of positive eigenvalues $r_{\mathbf{n}}$ may be different for different direction \mathbf{n} . We call such system a *linear symmetric hyperbolic system with paired eigenvalues*. We denote the (orthogonal) eigenvalue decomposition of $\mathbf{B}_{\mathbf{n}}$ as

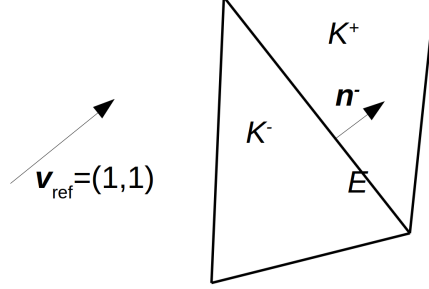
$$\mathbf{B}_{\mathbf{n}} = \mathbf{S}_{\mathbf{n}} \mathbf{\Lambda}_{\mathbf{n}} \mathbf{S}_{\mathbf{n}}^{-1}, \quad (3.3a)$$

with the eigenvalues in the diagonal matrix in descending order

$$\mathbf{\Lambda}_{\mathbf{n}} := \text{diag}([\lambda_{\mathbf{n},1}^+, \dots, \lambda_{\mathbf{n},r_{\mathbf{n}}}^+, 0, \dots, 0, \lambda_{\mathbf{n},r_{\mathbf{n}}}^-, \dots, \lambda_{\mathbf{n},1}^-]). \quad (3.3b)$$

We then give examples including the advection, acoustics, aeroacoustics, electromagnetism, and elastodynamics that shall fit into the framework. The key idea follows from the one-dimensional case by adding auxiliary *zero* equations to the system so that we get a system with paired eigenvalues.

FIGURE 1. Illustration of the choice of direction for an edge E shared by two triangles K^- and K^+



3.1. Notation and definitions in the two-dimensional case. Let $\Omega_h = \{K\}$ denote a conforming triangulation of Ω with shape-regular triangular/rectangular elements K , and set $\partial\Omega_h = \{\partial K : K \in \Omega_h\}$ where ∂K is the boundary of the element K . Denote \mathcal{E}_h be the collection of edges in the mesh Ω_h . For each $K \in \Omega_h$, we denote by h_K the diameter of K and set, as usual, $h = \max_{K \in \Omega_h} h_K$. The finite element space associated with the mesh Ω_h is of the form

$$V_h^k := \{v \in L^2(\Omega) : v|_K \in V_k(K) \quad \forall K \in \Omega_h\},$$

where

$$V_k(K) = \begin{cases} P^k(K) & \text{if } K \text{ is a triangle,} \\ Q^k(K) & \text{if } K \text{ is a rectangle,} \end{cases}$$

and $P^k(K)$ is the space of polynomials of degrees at most k on K , and $Q^k(K)$ is the tensor product of polynomials of degrees at most k in each variable.

We would like to adopt the following notation for the average and jumps of any function ϕ_h in the DG space V_h^k . Let $E \in \mathcal{E}_h$ be an edge shared by two elements K^+ and K^- . Let $\mathbf{n}^\pm = (n_x^\pm, n_y^\pm)$ be the normal direction on E from K^\pm . We select the unique element K^- such that the direction $\mathbf{n}^- = (n_x^-, n_y^-)$ satisfies

$$\mathbf{v}_{\text{ref}} \cdot \mathbf{n}^- \geq 0, \quad (\text{when } \mathbf{v}_{\text{ref}} \cdot \mathbf{n}^- = 0 \text{ we take } \mathbf{n}^- \text{ such that } n_x^- > 0), \quad (3.4)$$

where $\mathbf{v}_{\text{ref}} = (1, 1)$ is an *artificial (velocity) vector* used to single out the unique K^- . See an illustration in Figure 1. Let $(\phi_h)^\pm = (\phi_h)|_{K^\pm}$. We use

$$[[\phi_h]]|_E = \phi_h^+ - \phi_h^-, \quad \{\{\phi_h\}\}|_E = \frac{1}{2}(\phi_h^+ + \phi_h^-) \quad (3.5)$$

to denote the jump and the average of ϕ_h on the edge E . We shall always take \mathbf{n}^- as the normal direction of the edge E .

3.2. Energy-conserving DG methods for linear symmetric hyperbolic systems with paired eigenvalues. Following the one-dimensional case (2.33), the energy-conserving semi-discrete DG methods for the linear symmetric hyperbolic systems (3.1) with paired eigenvalues is given as follows. Find, for any time

$t \in (0, T]$, the unique function $\mathbf{u}_h = \mathbf{u}_h(t) \in [V_h^k]^m$ such that

$$\begin{aligned} \int_K \mathbf{B}_0(\mathbf{u}_h)_t \cdot \mathbf{v}_h d\mathbf{x} - \int_K \mathbf{B}_1 \mathbf{u}_h \cdot (\mathbf{v}_h)_x d\mathbf{x} - \int_K \mathbf{B}_2 \mathbf{u}_h \cdot (\mathbf{v}_h)_y d\mathbf{x} \\ + \int_{\partial K} \widehat{\mathbf{B}_n \mathbf{u}_h} \cdot \mathbf{v}_h ds = 0 \end{aligned} \quad (3.6)$$

holds for all $\mathbf{v}_h \in [V_h^k]^m$ and all $K \in \Omega_h$. Here, the numerical flux, which is similar to the one-dimensional case (2.33b), is given as follows:

$$\widehat{\mathbf{B}_{n^-} \mathbf{u}_h}|_E = \mathbf{B}_{n^-} \{\{\mathbf{u}_h\}\} + \frac{1}{2} \sum_{\mu=1}^{r_n} \sqrt{|\lambda_{n^-, \mu}^+ \lambda_{n^-, \mu}^-|} \mathbf{S}_{n^-} \mathbf{R}_\mu \mathbf{S}_{n^-}^{-1} \llbracket \mathbf{u}_h \rrbracket, \quad (3.7a)$$

$$\widehat{\mathbf{B}_{n^+} \mathbf{u}_h}|_E = -\widehat{\mathbf{B}_{n^-} \mathbf{u}_h}|_E, \quad (3.7b)$$

where \mathbf{n}^- is the direction of the edge E that satisfy (3.4), and $\mathbf{n}^+ = -\mathbf{n}^-$ is the direction with opposite sign.

Recall that the matrix $\mathbf{R}_\mu \in \mathbb{R}^{m \times m}$ is the anti-symmetric matrix that only has non-vanishing components on the $(\mu, m - \mu)$ and $(m - \mu, \mu)$ locations, with

$$\mathbf{R}_\mu(\mu, m - \mu) = 1, \quad \mathbf{R}_\mu(m - \mu, \mu) = -1.$$

Note that the above choice of numerical flux is consistent and conservative.

Remark 3.1 (On the numerical flux). Recall that the (dissipative) upwinding numerical flux is given by

$$\widehat{\mathbf{B}_{n^-} \mathbf{u}_h}|_E = \mathbf{B}_{n^-} \{\{\mathbf{u}_h\}\} - \frac{1}{2} \mathbf{S}_{n^-} |\mathbf{\Lambda}_{n^-}| \mathbf{S}_{n^-}^{-1} \llbracket \mathbf{u}_h \rrbracket, \quad (3.8)$$

where

$$|\mathbf{\Lambda}_{n^+}| = \text{diag}(|\lambda_{n^-, 1}^+|, \dots, |\lambda_{n^-, r_n}^+|, 0, \dots, 0, |\lambda_{n^-, r_n}^-|, \dots, |\lambda_{n^-, 1}^-|).$$

It is obtained by solving the Riemann problem along the normal direction. The cheaper-to-implement, more dissipative Lax-Friedrichs flux is given by

$$\widehat{\mathbf{B}_{n^-} \mathbf{u}_h}|_E = \mathbf{B}_{n^-} \{\{\mathbf{u}_h\}\} - \frac{1}{2} \max\{|\lambda_{n^-, 1}^+|, |\lambda_{n^-, 1}^-|\} \llbracket \mathbf{u}_h \rrbracket, \quad (3.9)$$

and the central flux is given by

$$\widehat{\mathbf{B}_{n^-} \mathbf{u}_h}|_E = \mathbf{B}_{n^-} \{\{\mathbf{u}_h\}\}. \quad (3.10)$$

The only difference among these numerical fluxes is on the choice of the *stabilization* term involving $\llbracket \mathbf{u}_h \rrbracket$.

We have energy-conservation of the method (3.6), just as the one-dimensional case. The proof is identical, and is omitted.

Theorem 3.2. *Let $\mathbf{u}_h \in [V_h^k]^m$ be the numerical solution of the semi-discrete DG scheme (3.6). Then, the total energy*

$$E(t) = \int_{\Omega} (\mathbf{B}_0 \mathbf{u}_h) \cdot \mathbf{u}_h d\mathbf{x}$$

is conserved for all time.

Remark 3.3 (Doubling the unknowns). Any linear symmetric hyperbolic system (3.1) can be modified to be a system with paired eigenvalues, essentially following the doubling the unknowns approach in section 2.3. In particular, we shall consider the following augmented system:

$$\mathbf{B}_0 \mathbf{u}_t + \mathbf{B}_1 \mathbf{u}_x + \mathbf{B}_2 \mathbf{u}_y = 0, \quad (3.11a)$$

$$\mathbf{B}_0 \phi_t - \mathbf{B}_1 \phi_x - \mathbf{B}_2 \phi_y = 0, \quad (3.11b)$$

where the auxiliary *zero* variable $\phi(x, y, t)$ has a *zero* initial condition. It is easy to observe that the above system is a system with paired eigenvalues. Taking into account its block anti-symmetric structure, the scheme (3.6) applied to the equations (3.11) has the following form. Find, for any time $t \in (0, T]$, the unique function $(\mathbf{u}_h, \phi_h) \in [V_h^k]^m \times [V_h^k]^m$ such that

$$\begin{aligned} \int_K \mathbf{B}_0(\mathbf{u}_h)_t \cdot \mathbf{v}_h \, d\mathbf{x} - \int_K \mathbf{B}_1 \mathbf{u}_h \cdot (\mathbf{v}_h)_x \, d\mathbf{x} - \int_K \mathbf{B}_2 \mathbf{u}_h \cdot (\mathbf{v}_h)_y \, d\mathbf{x} \\ + \int_{\partial K} \widehat{\mathbf{B}_n \mathbf{u}_h} \cdot \mathbf{v}_h \, ds = 0, \end{aligned} \quad (3.12a)$$

$$\begin{aligned} \int_K \mathbf{B}_0(\phi_h)_t \cdot \psi_h \, d\mathbf{x} + \int_K \mathbf{B}_1 \phi_h \cdot (\psi_h)_x \, d\mathbf{x} + \int_K \mathbf{B}_2 \phi_h \cdot (\psi_h)_y \, d\mathbf{x} \\ - \int_{\partial K} \widehat{\mathbf{B}_n \phi_h} \cdot \psi_h \, ds = 0, \end{aligned} \quad (3.12b)$$

holds for all $(\mathbf{v}_h, \psi_h) \in [V_h^k]^m \times [V_h^k]^m$ and all $K \in \Omega_h$, with the numerical fluxes given as follows:

$$\widehat{\mathbf{B}_{n^-} \mathbf{u}_h}|_E = \mathbf{B}_{n^-} \{ \{ \mathbf{u}_h \} \} + \frac{1}{2} |\mathbf{B}_{n^-}| [\phi_h], \quad (3.12c)$$

$$\widehat{\mathbf{B}_{n^-} \phi_h}|_E = \mathbf{B}_{n^-} \{ \{ \phi_h \} \} + \frac{1}{2} |\mathbf{B}_{n^-}| [\mathbf{u}_h], \quad (3.12d)$$

$$\widehat{\mathbf{B}_{n^+} \mathbf{u}_h}|_E = -\widehat{\mathbf{B}_{n^-} \mathbf{u}_h}|_E, \quad \widehat{\mathbf{B}_{n^+} \phi_h}|_E = -\widehat{\mathbf{B}_{n^-} \phi_h}|_E, \quad (3.12e)$$

where $|\mathbf{B}_{n^-}| = \mathbf{S}_{n^-} |\mathbf{\Lambda}_{n^-}| \mathbf{S}_{n^-}^{-1}$. It is interesting to see the similarity of this numerical flux with the upwinding flux (3.8). Unlike the upwinding case, the jump term in the above numerical flux do not contribute to dissipation, but to the *coupling* of the primal variables \mathbf{u}_h and the auxiliary variables ϕ_h . Note also that the above numerical flux is different from the one dimensional case in Remark 2.9 as we need the eigenvalue decomposition of \mathbf{B}_{n^-} for the numerical flux. We numerically observed that on triangular meshes, such eigenvalue decomposition is crucial for the method to be optimally convergent.

Finally we point out that doubling the unknowns essentially leads to a doubling of the computational cost when explicit time-stepping schemes, see section (2.6), are used.

Remark 3.4 (Error estimates). The error analysis of the method (3.6) is more involved than the 1D case. Suboptimal convergence order of k can be proven using a standard L^2 -projection on general mesh. Optimal convergence order of $k + 1$ for all the variables \mathbf{u}_h on rectangular meshes can be proven by using the super-convergence result of Lesaint and Raviart [18] of the tensor-product Gauss-Radau projection, see also [7, Lemma 3.6]. However, the method is numerically observed to be suboptimal for certain hyperbolic systems on general triangular meshes including acoustics with zero background velocity (Example 4.10 in section 4) and

elastodynamics (Example 4.11 in section 4). It was also numerically observed in [25] to be suboptimal for the DG method with an alternating numerical flux for the time domain Maxwell's equation on triangular meshes, which is equivalent to the method (3.6) directly applied to the Maxwell's equations (see section 3.3.4). We note that the aforementioned equations are by themselves systems with paired eigenvalues. On the other hand, the doubling unknowns approach (3.12) in Remark 3.3 applied to the augmented system is numerically observed to be optimally convergent for the aforementioned equations. Of course, we have also doubled the computational cost. Further study needs to be conducted to understand the convergence behavior of this method on triangular meshes.

Remark 3.5 (Time discretization, source term, and boundary conditions). The same high-order energy-conserving Lax-Wendroff time discretization (2.40) can be used for (3.6) to get a fully discrete energy-conserving DG method. We can also use the Runge-Kutta type Lax-Wendroff time discretization (2.41). Source terms and boundary conditions can be easily incorporated into the scheme (3.6). We refer details to the discussion in section 2.6 and section 2.7.

3.3. Practical examples. Now, we consider the application of Theorem 3.2 and Remark 3.3 for a large class of symmetric linear hyperbolic system of equations.

3.3.1. Advection. We consider the advection equation

$$u_t + b_0 u_x + b_1 u_y = 0, \quad (3.13)$$

with $b_0^2 + b_1^2 \neq 0$. Following Remark 3.3, we convert it to a system with paired eigenvalues by introducing the auxiliary *zero* function $\phi(x, y, t)$ that solve the equation

$$\phi_t - b_0 \phi_x - b_1 \phi_y = 0.$$

The energy-conserving numerical flux (3.7) for the resulting system on the edge E with normal direction $\mathbf{n} = (n_x, n_y)$ is given by

$$\widehat{\mathbf{B}_n \mathbf{u}_h}|_E = \begin{bmatrix} b_n \{u_h\} \\ -b_n \{\phi_h\} \end{bmatrix} + \frac{1}{2} \begin{bmatrix} |b_n| \llbracket \phi_h \rrbracket \\ -|b_n| \llbracket u_h \rrbracket \end{bmatrix}, \quad (3.14)$$

where $b_n = b_0 n_x + b_1 n_y$ is the normal velocity. We mention in particular that the above numerical flux is independent of the artificial direction $\mathbf{v}_{\text{ref}} = (1, 1)$ used to determine the unique direction of the edge E in (3.4).

3.3.2. Acoustics. We consider the acoustics equations

$$\begin{bmatrix} p \\ u \\ v \end{bmatrix}_t + \begin{bmatrix} u_0 & K_0 & 0 \\ 1/\rho_0 & u_0 & 0 \\ 0 & 0 & u_0 \end{bmatrix} \begin{bmatrix} p \\ u \\ v \end{bmatrix}_x + \begin{bmatrix} v_0 & 0 & K_0 \\ 0 & v_0 & 0 \\ 1/\rho_0 & 0 & v_0 \end{bmatrix} \begin{bmatrix} p \\ u \\ v \end{bmatrix}_y = 0, \quad (3.15)$$

where $p(x, y, t)$ is the pressure, and $\vec{u} = (u(x, y, t), v(x, y, t))$ is the velocity vector, and for the constants, $\vec{u}_0 = (u_0, v_0)$ is the velocity for a background flow, $K_0 > 0$ is the bulk modulus of compressibility and $\rho_0 > 0$ is the density.

Similar to the one-dimensional case in Section 2.4, the system can be symmetrized to the following form:

$$\underbrace{\begin{bmatrix} 1/K_0 & 0 & 0 \\ 0 & \rho_0 & 0 \\ 0 & 0 & \rho_0 \end{bmatrix}}_{:=\mathbf{B}_0} \begin{bmatrix} p \\ u \\ v \end{bmatrix}_t + \underbrace{\begin{bmatrix} u_0/K_0 & 1 & 0 \\ 1 & u_0\rho_0 & 0 \\ 0 & 0 & u_0\rho_0 \end{bmatrix}}_{:=\mathbf{B}_1} \begin{bmatrix} p \\ u \\ v \end{bmatrix}_x + \underbrace{\begin{bmatrix} v_0/K_0 & 0 & 1 \\ 0 & v_0\rho_0 & 0 \\ 1 & 0 & v_0\rho_0 \end{bmatrix}}_{:=\mathbf{B}_2} \begin{bmatrix} p \\ u \\ v \end{bmatrix}_y = 0, \quad (3.16)$$

The doubling unknowns approach in Remark 3.3 shall be used for the system (3.16) on general triangular meshes. However, we can save the computational cost by looking into the eigenvalue structure of the matrix $\mathbf{B}_n = n_x\mathbf{B}_1 + n_y\mathbf{B}_2$. The following discussion is similar to the one dimensional case in section 2.4. We mention that the following simplification shall be done on Cartesian meshes, as we numerically observe suboptimal convergence of this simplified method on general triangular meshes.

The matrix \mathbf{B}_n is given by

$$\mathbf{B}_n := \begin{bmatrix} v_n/K_0 & n_x & n_y \\ n_x & v_n\rho_0 & 0 \\ n_y & 0 & v_n\rho_0 \end{bmatrix},$$

where $v_n = u_0n_x + v_0n_y$. It has an eigenvalue $\lambda_1 = v_n\rho_0$, and a pair of eigenvalues λ_2^\pm that are the two roots of the following quadratic equation

$$\lambda^2 - (v_n/K_0 + v_n/K_0)\lambda + v_n^2/c_0^2 - 1 = 0$$

where $c_0 = \sqrt{K_0/\rho_0}$ is the speed of sound. We shall distinguish with the following three cases.

Zero background velocity ($\vec{u}_0 = 0$). In this case ($u_0 = v_0 = 0$), the three eigenvalues of \mathbf{B}_n are $0, \pm 1$. The system (3.16) by itself is a linear symmetric hyperbolic system with paired eigenvalues. We can direct apply the method (3.6) to the equations (3.16). The numerical flux of the method is noting but the alternating numerical flux considered in [5]:

$$\widehat{\mathbf{B}_n \mathbf{u}_h}|_E = \begin{bmatrix} u_h^+ n_x + v_h^+ n_y \\ p_h^- n_x \\ p_h^- n_y \end{bmatrix}. \quad (3.17)$$

This method is numerically observed to be suboptimal on general triangular meshes.

Subsonic case ($0 < u_0^2 + v_0^2 < c_0^2$). In this case, the magnitude of the normal velocity $v_n = u_0n_x + v_0n_y$ on any edge E is less than c_0 , and in general is not equal to zero. In this case, the matrix \mathbf{B}_n either has 2 positive eigenvalues and 1 negative eigenvalue ($v_n > 0$) or has 1 positive eigenvalues and 2 negative eigenvalue ($v_n < 0$). We can convert the system (3.16) to a 4-component linear symmetric system with paired eigenvalues by introducing the *zero* function $\phi(x, y, t)$ that solves

$$\rho_0\phi_t - \rho_0u_0\phi_x - \rho_0v_0\phi_y = 0.$$

The resulting system reads

$$\begin{aligned}
& \underbrace{\begin{bmatrix} 1/K_0 & 0 & 0 & 0 \\ 0 & \rho_0 & 0 & 0 \\ 0 & 0 & \rho_0 & 0 \\ 0 & 0 & 0 & \rho_0 \end{bmatrix}}_{:=\widetilde{\mathbf{B}}_0} \begin{bmatrix} p \\ u \\ v \\ \phi \end{bmatrix}_t + \underbrace{\begin{bmatrix} u_0/K_0 & 1 & 0 & 0 \\ 1 & u_0\rho_0 & 0 & 0 \\ 0 & 0 & u_0\rho_0 & 0 \\ 0 & 0 & 0 & -u_0\rho_0 \end{bmatrix}}_{:=\widetilde{\mathbf{B}}_1} \begin{bmatrix} p \\ u \\ v \\ \phi \end{bmatrix}_x \\
& + \underbrace{\begin{bmatrix} v_0/K_0 & 0 & 1 & 0 \\ 0 & v_0\rho_0 & 0 & 0 \\ 1 & 0 & v_0\rho_0 & 0 \\ 0 & 0 & 0 & -v_0\rho_0 \end{bmatrix}}_{:=\widetilde{\mathbf{B}}_2} \begin{bmatrix} p \\ u \\ v \\ \phi \end{bmatrix}_y = 0,
\end{aligned} \tag{3.18}$$

It is easy to verify that the matrix $\widetilde{\mathbf{B}}_{\mathbf{n}} = \widetilde{\mathbf{B}}_1 n_x + \widetilde{\mathbf{B}}_2 n_y$ always has paired eigenvalues for the above system for any normal direction \mathbf{n} .

Denoting the 4-component vector $\widetilde{\mathbf{u}}_h = [p_h, u_h, v_h, \phi_h]'$, the numerical flux on the edge E for the system (3.18) reads

$$\widetilde{\mathbf{B}}_{\mathbf{n}} \widetilde{\mathbf{u}}_h|_E = \begin{bmatrix} v_n/K_0 \{p_h\} + \{u_h\} n_x + \{v_h\} n_y \\ \{p_h\} n_x + v_n \rho_0 \{u_h\} \\ \{p_h\} n_y + v_n \rho_0 \{v_h\} \\ -v_n \rho_0 \{\phi_h\} \end{bmatrix} + \frac{1}{2} \begin{bmatrix} \alpha_n (\llbracket u_h \rrbracket n_x + \llbracket v_h \rrbracket n_y) \\ -\alpha_n \llbracket p_h \rrbracket n_x - \beta_n \llbracket \phi_h \rrbracket n_y \\ -\alpha_n \llbracket p_h \rrbracket n_y + \beta_n \llbracket \phi_h \rrbracket n_x \\ \beta_n (\llbracket u_h \rrbracket n_y - \llbracket v_h \rrbracket n_x) \end{bmatrix}, \tag{3.19}$$

where $\alpha_n = \sqrt{1 - v_n^2/c_0^2}$ and $\beta_n = |v_n|$. Different from the zero background velocity case, this method is numerically observed to be optimal on general triangular meshes.

Supersonic case $u_0^2 + v_0^2 \geq c_0^2$. In this case, there exists direction \mathbf{n} such that all eigenvalues of the matrix $\mathbf{B}_{\mathbf{n}}$ are positive. We shall use the doubling the unknowns approach in Remark 3.3, and consider the augmented 6-component system.

3.3.3. Linearized Euler equations. We consider the linearized Euler equations in dimensionless form

$$\begin{bmatrix} \rho \\ u \\ v \\ p \end{bmatrix}_t + \begin{bmatrix} M_x & 1 & 0 & 0 \\ 0 & M_x & 0 & 1 \\ 0 & 0 & M_x & 0 \\ 0 & 1 & 0 & M_x \end{bmatrix} \begin{bmatrix} \rho \\ u \\ v \\ p \end{bmatrix}_x + \begin{bmatrix} M_y & 0 & 1 & 0 \\ 0 & M_y & 0 & 0 \\ 0 & 0 & M_y & 1 \\ 0 & 0 & 1 & M_y \end{bmatrix} \begin{bmatrix} \rho \\ u \\ v \\ p \end{bmatrix}_y = 0, \tag{3.20}$$

where $M_x, M_y \geq 0$ with are the constant mean flow Mach number in the x - and y -direction, respectively. Subtracting the first equation by the fourth, one obtain

the following linear symmetric system for the unknown vector $\mathbf{u} := [\rho - p, u, v, p]'$:

$$\begin{aligned} \begin{bmatrix} \rho - p \\ u \\ v \\ p \end{bmatrix}_t + \underbrace{\begin{bmatrix} M_x & 0 & 0 & 0 \\ 0 & M_x & 0 & 1 \\ 0 & 0 & M_x & 0 \\ 0 & 1 & 0 & M_x \end{bmatrix}}_{:=\mathbf{B}_1} \begin{bmatrix} \rho - p \\ u \\ v \\ p \end{bmatrix}_x \\ + \underbrace{\begin{bmatrix} M_y & 0 & 0 & 0 \\ 0 & M_y & 0 & 0 \\ 0 & 0 & M_y & 1 \\ 0 & 0 & 1 & M_y \end{bmatrix}}_{:=\mathbf{B}_2} \begin{bmatrix} \rho - p \\ u \\ v \\ p \end{bmatrix}_y = 0. \end{aligned} \quad (3.21)$$

Note that the above equation is simply the combination of the acoustic equations for $[u, v, p]$, and the advection equation for $\rho - p$. We can just follow the discussion on the previous two subsections to obtain the energy-conserving method. We leave out the details.

3.3.4. Electromagnetism. We consider the two-dimensional time-domain Maxwell equations in transverse magnetic form (TM) in a heterogeneous media

$$\begin{bmatrix} \mu H^x \\ \mu H^y \\ \epsilon E^z \end{bmatrix}_t + \begin{bmatrix} 0 & 0 & 0 \\ 0 & 0 & -1 \\ 0 & -1 & 0 \end{bmatrix} \begin{bmatrix} H^x \\ H^y \\ E^z \end{bmatrix}_x + \begin{bmatrix} 0 & 0 & 1 \\ 0 & 0 & 0 \\ 1 & 0 & 0 \end{bmatrix} \begin{bmatrix} H^x \\ H^y \\ E^z \end{bmatrix}_y = 0, \quad (3.22)$$

where $(H^x(x, y, t), H^y(x, y, t))$ is the magnetic fields, and $E^z(x, y, t)$ is the electric field, and $\mu, \epsilon : \Omega \rightarrow \mathbb{R}$ is the magnetic permeability, and electric permittivity, respectively.

The system is similar to the acoustic case with *zero* background mean flow. On general triangular meshes, we propose to double the unknowns and obtain the DG method (3.12) for the 6-components augmented system. On Cartesian meshes, we can also directly apply the method (3.6) to (3.22) to obtain the DG method with an alternating numerical flux. The alternating flux DG method, which is optimal on Cartesian meshes but suboptimal on triangular meshes, was discussed in details recently [21, 25], where special focus was made on Maxwell's equations in Drude metamaterials.

3.3.5. Elastodynamics. We consider the elastodynamics equations in a heterogeneous, isotropic media, written in stress-velocity form

$$\begin{aligned} \begin{bmatrix} \sigma_{xx} \\ \sigma_{yy} \\ \sigma_{xy} \\ v \\ w \end{bmatrix}_t + \begin{bmatrix} 0 & 0 & 0 & -(\lambda + 2\mu) & 0 \\ 0 & 0 & 0 & -\lambda & 0 \\ 0 & 0 & 0 & 0 & -\mu \\ -1/\rho & 0 & 0 & 0 & 0 \\ 0 & 0 & -1/\rho & 0 & 0 \end{bmatrix} \begin{bmatrix} \sigma_{xx} \\ \sigma_{yy} \\ \sigma_{xy} \\ v \\ w \end{bmatrix}_x \\ + \begin{bmatrix} 0 & 0 & 0 & 0 & -\lambda \\ 0 & 0 & 0 & 0 & -(\lambda + 2\mu) \\ 0 & 0 & 0 & -\mu & 0 \\ 0 & 0 & -1/\rho & 0 & 0 \\ 0 & -1/\rho & 0 & 0 & 0 \end{bmatrix} \begin{bmatrix} \sigma_{xx} \\ \sigma_{yy} \\ \sigma_{xy} \\ v \\ w \end{bmatrix}_y = 0, \end{aligned} \quad (3.23)$$

where $\boldsymbol{\sigma} = \begin{bmatrix} \sigma_{xx} & \sigma_{xy} \\ \sigma_{xy} & \sigma_{yy} \end{bmatrix}$ is the stress field, and $\mathbf{v} = [v, w]'$ is the velocity field, and λ and μ are the Lamé constants, and ρ is the density functions. We assume λ, μ, ρ are piecewise constants with discontinuity aligned with the mesh. The system (3.23) can be transformed into a symmetric hyperbolic system by left multiplying the equation with the symmetric positive definite matrix

$$\mathbf{B}_0 := \begin{bmatrix} \frac{\lambda+2\mu}{4\mu(\mu+\lambda)} & \frac{-\lambda}{4\mu(\mu+\lambda)} & 0 & 0 & 0 \\ \frac{-\lambda}{4\mu(\mu+\lambda)} & \frac{\lambda+2\mu}{4\mu(\mu+\lambda)} & 0 & 0 & 0 \\ 0 & 0 & \frac{1}{\mu} & 0 & 0 \\ 0 & 0 & 0 & \rho & 0 \\ 0 & 0 & 0 & 0 & \rho \end{bmatrix}.$$

Denoting the 5-component vector $\mathbf{u} = [\sigma_{xx}, \sigma_{yy}, \sigma_{xy}, v, w]'$, and the matrices

$$\mathbf{B}_1 = \begin{bmatrix} 0 & 0 & 0 & -1 & 0 \\ 0 & 0 & 0 & 0 & 0 \\ 0 & 0 & 0 & 0 & -1 \\ -1 & 0 & 0 & 0 & 0 \\ 0 & 0 & -1 & 0 & 0 \end{bmatrix}, \quad \mathbf{B}_2 = \begin{bmatrix} 0 & 0 & 0 & 0 & 0 \\ 0 & 0 & 0 & 0 & -1 \\ 0 & 0 & 0 & -1 & 0 \\ 0 & 0 & -1 & 0 & 0 \\ 0 & -1 & 0 & 0 & 0 \end{bmatrix}$$

We have

$$\mathbf{B}_0 \mathbf{u}_t + \mathbf{B}_1 \mathbf{u}_x + \mathbf{B}_2 \mathbf{u}_y = 0. \quad (3.24)$$

The matrix $\mathbf{B}_n = \mathbf{B}_1 n_x + \mathbf{B}_2 n_y$ has two positive eigenvalues $\sqrt{1 \pm n_x n_y}$, and two negative eigenvalues $-\sqrt{1 \pm n_x n_y}$, and a zero eigenvalue. Hence, the system (3.23) is already a symmetric system with paired eigenvalues.

Similar to the electromagnetism case in section 3.3.4, we propose to double the unknowns and obtain the DG method (3.12) for the 10-component augmented system on general triangular meshes. On Cartesian meshes, we directly apply the method (3.6) to the equations (3.24) to obtain the DG method with

$$\widehat{\mathbf{B}_n \mathbf{u}_h}|_E = \begin{bmatrix} -n_x v_h^+ \\ -n_y w_h^+ \\ -n_y v_h^+ - n_x w_h^+ \\ -n_x \sigma_{xx,h}^- - n_y \sigma_{xy,h}^- \\ -n_x \sigma_{xy,h}^- - n_y \sigma_{yy,h}^- \end{bmatrix}.$$

For an efficient time integration, we prefer to work directly with the (equivalent) original stress-velocity form (3.23). This leads to a diagonal mass matrix for the whole system if the orthogonal basis is used.

4. NUMERICAL RESULTS

We present extensive numerical results to assess the performance of the proposed energy-conserving DG method. We also compare results with the (dissipative) upwinding DG methods, and the (energy-conserving) DG methods with a central flux. All numerical simulation are performed using the open-source finite-element software NGSolve [24], <https://ngsolve.org/>.

For all the accuracy tests, we restrict ourselves to the spatial error, and take the 6-stage 6th order ($r = 6$) Lax-Wendroff time stepping (2.41) with a small enough time step size so that the temporal error can be neglected.

Example 4.1: 1D advection with periodic boundary condition. We consider the following advection equation

$$u_t + u_x = 0 \quad (4.1)$$

on a unit interval $I = [0, 1]$ with initial condition $u(x, 0) = \sin(2\pi x)$, and a periodic boundary condition. The exact solution is

$$u(x, t) = \sin(2\pi(x - t)).$$

We present numerical results with the following three DG methods:

- (U) the DG method for (4.1) with an upwinding numerical flux.
- (C) the DG method for (4.1) with a central numerical flux.
- (A) the DG method (2.10) with numerical flux (2.12) for the augmented system (2.9).

Table 4.1 lists the numerical errors and their orders for the above three DG methods at $T = 0.5$. We use P^k polynomials with $0 \leq k \leq 4$ on a nonuniform mesh which is a 10% random perturbation of the uniform mesh.

From the table we conclude that, one can always observe optimal $(k + 1)$ th order of accuracy for both the variable u_h (which approximate the solution u) and ϕ_h (which approximate the *zero* function) for the new energy-conserving DG method (2.10). This validates our convergence result in Theorem 2.7. Moreover, the absolute value of the error is slightly smaller than the optimal-convergent upwinding DG method for all polynomial degrees. We also observe suboptimal convergence for the (energy-conserving) DG method with a central flux for all polynomial degree. We specifically point out that while optimal convergence for the central DG method has been proven for even polynomial degrees on uniform meshes [9], Table 4.1 shows that such optimality no longer holds on nonuniform meshes, regardless of the polynomial degree.

Example 4.2: 1D advection with inflow boundary condition. We consider the same problem as in Example 4.1, but with the inflow boundary condition at the left end

$$u(0, t) = \sin(-2\pi t).$$

We use the three DG methods considered in Example 4.1, again on a nonuniform mesh which is a 10% random perturbation of the uniform mesh. For the boundary treatment, the upwinding boundary numerical flux (2.46) is used for all three DG methods. The time integration takes into account the boundary source term; see (2.43c). Table 4.2 lists the numerical errors and their orders with the three DG methods at $T = 0.5$. We observe similar convergence results as that for Example 4.1. We specifically mention that the Lax-Wendroff time integration (2.43c) do not leads to order reduction, which is typically observed for Runge-Kutta methods.

Example 4.3: 1D acoustics with periodic boundary condition. We consider the acoustic equation (2.20) with coefficients $\rho_0 = K_0 = 1, u_0 = 0.5$, i.e.,

$$\begin{aligned} p_t + .5p_x + u_x &= 0, \\ u_t + p_x + .5u_x &= 0. \end{aligned}$$

TABLE 4.1. The L^2 -errors and orders for Example 4.1 for the upwinding DG method (U), the central DG method (C), and the new DG method (A) on a random mesh of N cells. $T = 0.5$.

		(U)		(C)		(A)			
	N	$\ u - u_h\ $	Order	$\ u - u_h\ $	Order	$\ u - u_h\ $	Order	$\ \phi_h\ $	Order
P^0	10	5.22e-01	-0.00	3.16e-01	-0.00	1.40e-01	-0.00	2.06e-01	-0.00
	20	3.11e-01	0.75	1.70e-01	0.89	6.61e-02	1.08	1.10e-01	0.90
	40	1.74e-01	0.84	1.59e-01	0.10	3.25e-02	1.02	5.52e-02	1.00
	80	9.28e-02	0.90	1.09e-01	0.54	1.62e-02	1.01	2.76e-02	1.00
	160	4.76e-02	0.96	3.76e-02	1.54	8.10e-03	1.00	1.39e-02	0.99
P^1	10	1.88e-02	-0.00	4.72e-02	-0.00	1.06e-02	-0.00	1.47e-02	-0.00
	20	4.58e-03	2.04	2.21e-02	1.09	2.76e-03	1.94	3.64e-03	2.01
	40	1.11e-03	2.05	1.08e-02	1.03	6.75e-04	2.03	8.73e-04	2.06
	80	2.77e-04	2.00	5.40e-03	1.01	1.69e-04	1.99	2.18e-04	2.00
	160	6.89e-05	2.01	2.69e-03	1.00	4.22e-05	2.01	5.44e-05	2.00
P^2	10	9.22e-04	-0.00	1.05e-02	-0.00	6.03e-04	-0.00	7.04e-04	-0.00
	20	1.18e-04	2.97	1.49e-03	2.81	7.60e-05	2.99	8.94e-05	2.98
	40	1.43e-05	3.04	3.92e-04	1.92	9.25e-06	3.04	1.09e-05	3.03
	80	1.77e-06	3.02	6.90e-05	2.51	1.14e-06	3.02	1.35e-06	3.02
	160	2.23e-07	2.99	4.93e-06	3.81	1.44e-07	2.99	1.71e-07	2.98
P^3	10	3.64e-05	-0.00	1.93e-04	-0.00	2.37e-05	-0.00	2.66e-05	-0.00
	20	2.51e-06	3.86	1.05e-05	4.20	1.66e-06	3.84	1.87e-06	3.83
	40	1.47e-07	4.10	1.69e-06	2.63	9.71e-08	4.10	1.10e-07	4.09
	80	9.24e-09	3.99	1.63e-07	3.38	6.11e-09	3.99	6.92e-09	3.99
	160	5.71e-10	4.02	2.02e-08	3.01	3.78e-10	4.02	4.28e-10	4.01
P^4	10	1.22e-06	-0.00	3.76e-05	-0.00	8.29e-07	-0.00	9.20e-07	-0.00
	20	4.10e-08	4.90	1.34e-06	4.82	2.75e-08	4.91	3.04e-08	4.92
	40	1.20e-09	5.10	8.83e-08	3.92	8.04e-10	5.10	8.89e-10	5.10
	80	3.63e-11	5.04	3.67e-09	4.59	2.44e-11	5.04	2.70e-11	5.04
	160	1.17e-12	4.96	7.66e-11	5.58	7.87e-13	4.95	8.62e-13	4.97

The domain is a unit interval $I = [0, 1]$. The initial condition

$$p(x, 0) = \sin(2\pi x), u(x, 0) = 0,$$

and a periodic boundary condition is used. The exact solution is

$$p(x, t) = \frac{1}{2} \sin(2\pi(x - 1.5t)) + \frac{1}{2} \sin(2\pi(x + .5t)),$$

$$u(x, t) = \frac{1}{2} \sin(2\pi(x - 1.5t)) - \frac{1}{2} \sin(2\pi(x + .5t)).$$

We are in the subsonic regime, Theorem 2.13 indicates the energy-conserving DG method (2.24) with the numerical flux (2.24c) and (2.24d) using $\alpha_{j-\frac{1}{2}} = \frac{1}{2}\sqrt{0.75}$ is optimally convergent. We label this method as (A). Again, we also consider the numerical results for the DG method with the upwinding flux, labeled as (U), and with the central flux, labeled as (C).

Table 4.3 lists the numerical errors and their orders with the three DG methods at $T = 0.5$. Again, we observe optimal convergence for the DG method with

TABLE 4.2. The L^2 -errors and orders for Example 4.2 for the upwinding DG method (U), the central DG method (C), and the new DG method (A) on a random mesh of N cells. $T = 0.5$.

		(U)		(C)		(A)			
	N	$\ u - u_h\ $	Order	$\ u - u_h\ $	Order	$\ u - u_h\ $	Order	$\ \phi_h\ $	Order
P^0	10	4.54e-01	-0.00	3.27e-01	-0.00	1.89e-01	-0.00	2.45e-01	-0.00
	20	2.61e-01	0.80	1.58e-01	1.05	8.16e-02	1.21	1.15e-01	1.09
	40	1.46e-01	0.84	7.20e-02	1.13	3.63e-02	1.17	5.76e-02	1.00
	80	7.79e-02	0.90	4.81e-02	0.58	1.75e-02	1.05	2.86e-02	1.01
	160	3.99e-02	0.96	5.29e-02	-0.14	8.45e-03	1.05	1.41e-02	1.02
P^1	10	1.78e-02	-0.00	4.75e-02	-0.00	1.14e-02	-0.00	1.49e-02	-0.00
	20	4.38e-03	2.02	2.36e-02	1.01	2.73e-03	2.07	3.51e-03	2.09
	40	1.11e-03	1.98	1.14e-02	1.05	6.73e-04	2.02	8.67e-04	2.02
	80	2.76e-04	2.01	5.73e-03	1.00	1.68e-04	2.00	2.17e-04	2.00
	160	6.86e-05	2.01	2.87e-03	1.00	4.20e-05	2.00	5.43e-05	2.00
P^2	10	8.87e-04	-0.00	1.76e-03	-0.00	6.58e-04	-0.00	7.57e-04	-0.00
	20	1.20e-04	2.89	1.33e-04	3.72	8.04e-05	3.03	9.55e-05	2.99
	40	1.42e-05	3.08	1.66e-05	3.01	9.83e-06	3.03	1.17e-05	3.03
	80	1.78e-06	2.99	5.52e-06	1.59	1.20e-06	3.03	1.44e-06	3.03
	160	2.23e-07	2.99	4.34e-07	3.67	1.48e-07	3.02	1.73e-07	3.06
P^3	10	4.04e-05	-0.00	1.13e-04	-0.00	2.27e-05	-0.00	2.44e-05	-0.00
	20	2.13e-06	4.24	1.55e-05	2.86	1.47e-06	3.95	1.66e-06	3.88
	40	1.47e-07	3.86	1.84e-06	3.08	9.43e-08	3.96	1.07e-07	3.95
	80	8.84e-09	4.05	2.28e-07	3.01	5.85e-09	4.01	6.64e-09	4.01
	160	5.64e-10	3.97	2.81e-08	3.02	3.70e-10	3.98	4.20e-10	3.98
P^4	10	1.04e-06	-0.00	2.76e-06	-0.00	1.03e-06	-0.00	1.05e-06	-0.00
	20	3.65e-08	4.84	5.33e-08	5.70	2.52e-08	5.35	2.63e-08	5.32
	40	1.20e-09	4.93	3.65e-09	3.87	8.79e-10	4.84	9.32e-10	4.82
	80	3.69e-11	5.02	1.84e-10	4.31	2.52e-11	5.13	2.76e-11	5.08
	160	1.13e-12	5.02	4.04e-12	5.51	7.81e-13	5.01	8.64e-13	5.00

upwinding flux (U) and with the new energy-conserving flux (A), but suboptimal convergence for the DG method with central flux (C).

Similar numerical results, not reported here to save space, are also obtained for the supersonic case where the new method (A) shall solve an augmented system with 4 components.

Example 4.4: long time simulation: advection of a plane wave. We consider the advection equation (4.1) on the unit interval with periodic boundary condition and initial condition $u(x, 0) = \sin(6\pi x)$. The exact solution is

$$u(x, t) = \sin(6\pi(x - t)).$$

We use the above mentioned three DG methods using quadratic polynomials $k = 2$. Again, we denote the upwinding flux as (U), the central flux as (C), and the new method as (A). It is known that all three methods have optimally third-order convergence on uniform meshes. We take a uniform mesh with $N = 10$ cells, so there are 10 degrees of freedom per wavelength.

TABLE 4.3. The L^2 -error $(\|u - u_h\|^2 + \|p - p_h\|^2)^{1/2}$ and orders for Example 4.3 for the upwinding DG method (U), the central DG method (C), and the new DG method (A) on a random mesh of N cells. $T = 0.5$.

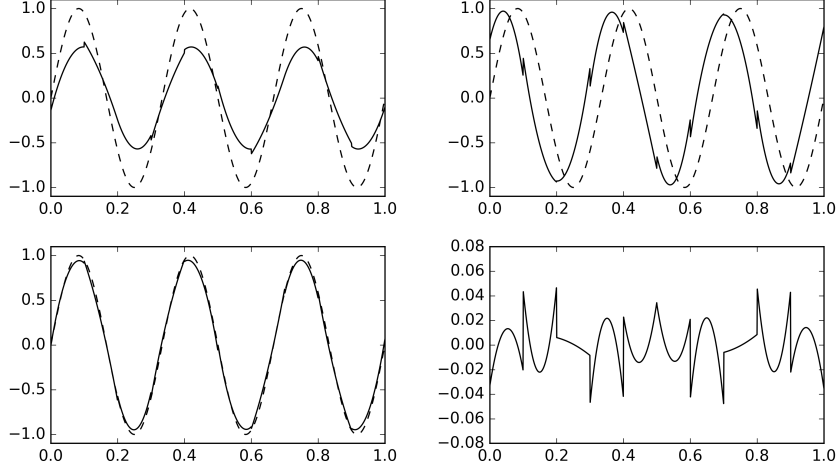
	N	(U)		(C)		(A)	
		Error	Order	Error	Order	Error	Order
P^0	10	5.04e-01	-0.00	3.64e-01	-0.00	3.08e-01	-0.00
	20	3.23e-01	0.64	2.26e-01	0.69	1.50e-01	1.04
	40	1.83e-01	0.82	1.52e-01	0.57	7.46e-02	1.01
	80	9.93e-02	0.88	1.07e-01	0.51	3.78e-02	0.98
	160	5.15e-02	0.95	3.47e-02	1.62	1.90e-02	0.99
P^1	10	1.94e-02	-0.00	5.00e-02	-0.00	2.56e-02	-0.00
	20	4.56e-03	2.09	2.22e-02	1.17	5.45e-03	2.23
	40	1.10e-03	2.05	1.08e-02	1.04	1.31e-03	2.06
	80	2.73e-04	2.02	5.35e-03	1.01	3.25e-04	2.01
	160	6.86e-05	1.99	2.68e-03	1.00	8.16e-05	2.00
P^2	10	8.96e-04	-0.00	1.18e-02	-0.00	1.26e-03	-0.00
	20	1.20e-04	2.90	2.14e-03	2.46	1.51e-04	3.06
	40	1.44e-05	3.06	3.71e-04	2.53	1.66e-05	3.19
	80	1.81e-06	2.99	6.52e-05	2.51	2.12e-06	2.97
	160	2.25e-07	3.01	4.10e-06	3.99	2.67e-07	2.99
P^3	10	3.76e-05	-0.00	2.01e-04	-0.00	4.79e-05	-0.00
	20	2.43e-06	3.95	1.02e-05	4.30	2.85e-06	4.07
	40	1.45e-07	4.07	1.67e-06	2.62	1.71e-07	4.06
	80	8.89e-09	4.03	1.59e-07	3.39	1.04e-08	4.03
	160	5.65e-10	3.98	2.01e-08	2.98	6.62e-10	3.98
P^4	10	1.18e-06	-0.00	4.10e-05	-0.00	1.36e-06	-0.00
	20	4.30e-08	4.78	1.97e-06	4.38	5.12e-08	4.73
	40	1.22e-09	5.14	8.35e-08	4.56	1.43e-09	5.16
	80	3.83e-11	4.99	3.46e-09	4.59	4.48e-11	5.00
	160	1.18e-12	5.02	6.52e-11	5.73	1.38e-12	5.02

For the time integration, we use the 3-stage, 3-rd order ($r = 3$) Lax-Wendroff time stepping (2.41), denoted as RK3. This is identical to the SSP-RK3 method, which is known to be dissipative. We also use the 3-stage, 4-th order ($r = 2$) energy-conserving, Lax-Wendroff time stepping (2.40), denoted as LF4, for the energy-conserving DG methods (C) and (A). The CFL number for all cases is taken to be 0.1.

The numerical results at time $T = 10$ (wave propagated 30 cycles) of the three DG methods using RK3 time stepping are shown in Figure 2. From this figure, we observe that the upwinding method (U) is very dissipative, the central method (C) is less dissipative but has a large phase error, while the new method (A) provides excellent results in terms of dissipation error and phase accuracy.

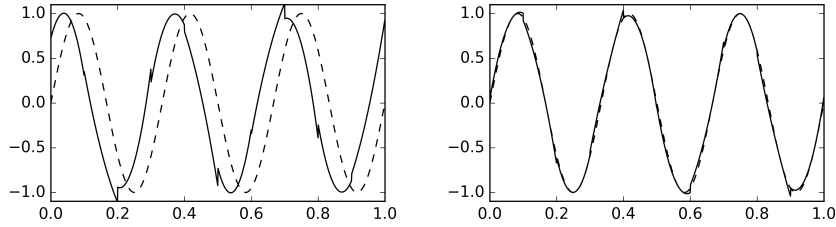
We also present the numerical results in Figure 3 for two energy-conserving methods (C) and (A) using the energy-conserving LF4 time integration. Numerical

FIGURE 2. Numerical solution at $T = 10$ for Example 4.4. RK3 time stepping. Top left: method (U). Top right: method (C). Bottom left: primal variable u_h for method (A). Bottom right: auxiliary variable ϕ_h for method (A). Solid line: numerical solution. Dashed line: exact solution. DG- P^2 space, 10 cells.



dissipation is not visible from the figures. But again, we observe large phase error for the central method (C), and small phase error for the new method (A).

FIGURE 3. Numerical solution at $T = 10$ for Example 4.4. LF4 time stepping. Left : method (C). Right: method (A) Solid line: numerical solution. Dashed line: exact solution. DG- P^2 space, 10 cells.



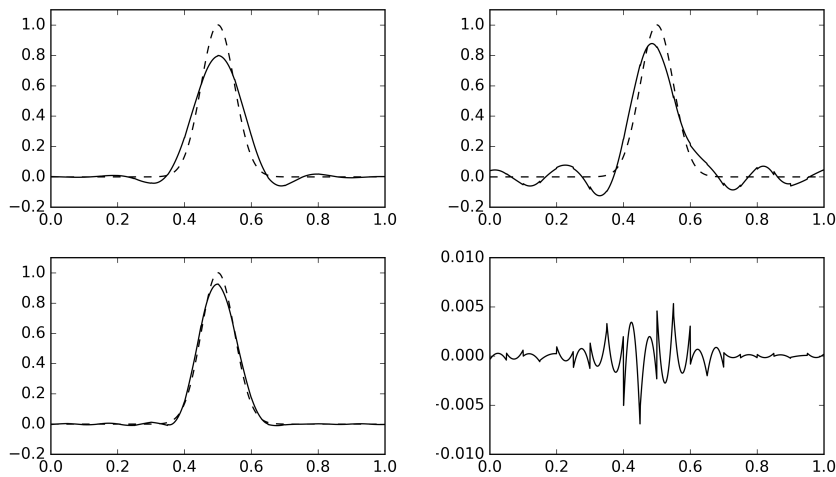
Example 4.5: long time simulation: advection of a Gaussian pulse. We consider the advection equation (4.1) on the unit interval with periodic boundary condition and initial condition $u(x, 0) = \exp(-200(x - .5)^2)$.

Again, we use the above mentioned three DG methods with quadratic polynomial space ($k = 2$). We take a uniform mesh with $N = 20$ cells, so there are a total of 60 degrees of freedom, which can roughly resolve waves frequency up to $k = 24\pi$.

The numerical results at time $T = 40$ (wave propagated 40 cycles) of the three DG methods using RK3 time stepping are shown in Figure 4. From this figure, we observe large dissipation error for the upwinding method (U), large dispersion error

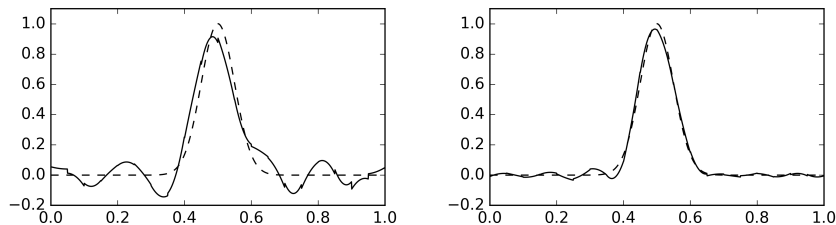
for the central method (C), and relatively the smallest dissipation and dispersion errors for the new method (A).

FIGURE 4. Numerical solution at $T = 40$ for Example 4.5. RK3 time stepping. Top left: method (U). Top right: method (C). Bottom left: primal variable u_h for method (A). Bottom right: auxiliary variable ϕ_h for method (A). Solid line: numerical solution. Dashed line: exact solution. DG- P^2 space, 20 cells.



We also present the numerical results at time $T = 40$ in Figure 3 for the two energy-conserving methods (C) and (A) using the energy-conserving LF4 time integration. This time, we observe a larger dispersion error for both methods, with the dissipation error for (A) slightly reduced.

FIGURE 5. Numerical solution at $T = 40$ for Example 4.6. LF4 time stepping. Left : method (C). Right: method (A) Solid line: numerical solution. Dashed line: exact solution. DG- P^2 space, 20 cells.



Example 4.6: long time simulation: spherical wave problem. This is our last one-dimensional example. We consider the following spherical wave problem, which was one of the benchmark problems proposed in the first computational aeroacoustics workshop [15],

$$u_t + u/r + u_r = 0$$

over the domain $5 \leq r \leq 450$, with initial condition $u(x, 0) = 0$. The boundary condition at $r = 5$ is

$$u(5, t) = \sin(\omega t), \quad \text{with } \omega = \pi/3.$$

Exact solution is

$$u(r, t) = \begin{cases} 0 & r > t + 5 \\ \frac{5}{r} [\sin(\omega(t - r + 5))] & r \leq t + 5. \end{cases}$$

Again, we use the above mentioned three DG methods with quadratic polynomial space ($k = 2$). Here we mention that although there is a source term in this equation, the auxiliary *zero* variable for the method (A) still solve the equation

$$\phi_t - \phi_r = 0.$$

We take a uniform mesh with $N = 250$ cells, so there are about 10 degrees of freedom per wavelength.

The numerical results at time $T = 400$ (wave propagated 50 cycles) along the segment $350 \leq r \leq 430$ of the three DG methods using RK3 time stepping are shown in Figure 6. From this figure, we observe large dissipation error for the upwinding method (U), large dissipation error and phase shift for the central method (C), and relatively the smallest dissipation error and phase shift for the new method (A).

Example 4.7: 2D advection with periodic boundary condition. We consider the following advection equation

$$u_t + u_x + u_y = 0 \tag{4.2}$$

on a unit square $\Omega = [0, 1] \times [0, 1]$ with initial condition $u(x, 0) = \sin(2\pi(x + y))$, and a periodic boundary condition. The exact solution is

$$u(x, t) = \sin(2\pi(x + y - 2t)).$$

We use the three DG methods, (U) for upwinding flux, (C) for central flux, and (A) for the new method in section 3.3.1. The methods are tested on both nonuniform rectangular meshes and unstructured triangular meshes; see Figure 7 for a coarse mesh. Table 4.4 lists the numerical errors and their orders for the above three DG methods at $T = 0.1$ on the rectangular meshes. And Table 4.5 lists the errors and orders on the triangular meshes. We use Q^k/P^k polynomials with $1 \leq k \leq 3$ for rectangular/triangular meshes.

From the tables, we observe optimal $(k + 1)$ th order of accuracy for both the variable u_h (which approximate the solution u) and ϕ_h (which approximate the *zero* function) for the new energy-conserving DG method (A). The optimal convergence on rectangular meshes is understood; see Remark 3.4. But we do not have a theoretical proof for such optimality on the triangular meshes. Similar to the 1D case in Example 4.1, the absolute value of the error for method (A) is slightly smaller than the optimal-convergent upwinding DG method (U) for all polynomial degree. We observe suboptimal convergence of order k for the method (C) for odd polynomial degree on both meshes. We also observe optimal convergence rate 3 for the method (C) using P^2 space on the triangular meshes, but a suboptimal convergence rate of about 2.5 on the nonuniform rectangular mesh.

FIGURE 6. Numerical solution for $350 \leq r \leq 430$ at $T = 400$ for Example 4.6. RK3 time stepping. Top: method (U). Middle: method (C). Bottom: method (A). Solid line: numerical solution. Dashed line: exact solution. DG- P^2 space, 250 cells.

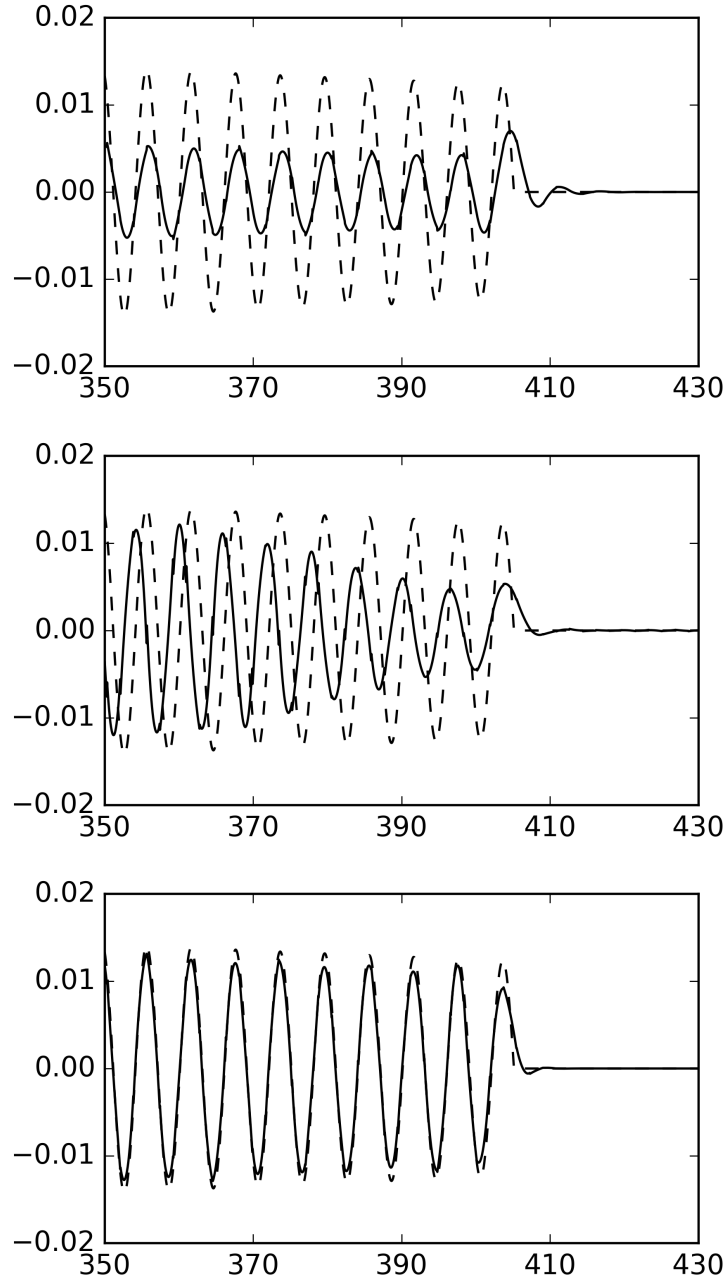


FIGURE 7. The coarse meshes. Left: nonuniform rectangular mesh. Right: unstructured triangular mesh.



TABLE 4.4. The L^2 -errors and orders for Example 4.7 for the upwinding DG method (U), the central DG method (C), and the new DG method (A) on a non-uniform rectangular mesh of $N \times N$ cells. $T = 0.1$.

	N	(U)		(C)		(A)			
		$\ u - u_h\ $	Order	$\ u - u_h\ $	Order	$\ u - u_h\ $	Order	$\ \phi_h\ $	Order
P^1	10	2.40e-02	-0.00	4.29e-02	-0.00	1.62e-02	-0.00	2.39e-02	-0.00
	20	6.15e-03	1.97	1.86e-02	1.21	3.85e-03	2.07	5.35e-03	2.16
	40	1.55e-03	1.99	8.88e-03	1.06	9.52e-04	2.02	1.26e-03	2.09
P^2	10	1.28e-03	-0.00	1.94e-03	-0.00	8.47e-04	-0.00	1.30e-03	-0.00
	20	1.61e-04	2.99	4.48e-04	2.12	1.05e-04	3.02	1.35e-04	3.27
	40	2.02e-05	3.00	8.04e-05	2.48	1.30e-05	3.01	1.53e-05	3.14
P^3	10	5.10e-05	-0.00	1.13e-04	-0.00	3.41e-05	-0.00	4.11e-05	-0.00
	20	3.25e-06	3.97	1.43e-05	2.98	2.16e-06	3.98	2.51e-06	4.03
	40	2.03e-07	4.00	1.77e-06	3.01	1.35e-07	4.00	1.55e-07	4.02

TABLE 4.5. The L^2 -errors and orders for Example 4.7 for the upwinding DG method (U), the central DG method (C), and the new DG method (A) on a unstructured triangular mesh with mesh size $h = 1/N$. $T = 0.1$.

	N	(U)		(C)		(A)			
		$\ u - u_h\ $	Order	$\ u - u_h\ $	Order	$\ u - u_h\ $	Order	$\ \phi_h\ $	Order
P^1	10	1.78e-02	-0.00	2.47e-01	-0.00	1.26e-02	-0.00	1.36e-02	-0.00
	20	4.63e-03	1.94	1.15e-01	1.10	3.16e-03	2.00	3.52e-03	1.95
	40	1.14e-03	2.02	5.20e-02	1.15	7.76e-04	2.02	8.46e-04	2.06
P^2	10	1.21e-03	-0.00	4.71e-03	-0.00	8.35e-04	-0.00	9.12e-04	-0.00
	20	1.50e-04	3.01	5.19e-04	3.18	1.02e-04	3.03	1.09e-04	3.06
	40	1.83e-05	3.04	6.24e-05	3.05	1.24e-05	3.04	1.34e-05	3.03
P^3	10	6.45e-05	-0.00	1.06e-03	-0.00	4.40e-05	-0.00	4.67e-05	-0.00
	20	4.27e-06	3.92	1.02e-04	3.37	2.93e-06	3.91	3.13e-06	3.90
	40	2.36e-07	4.18	1.17e-05	3.13	1.62e-07	4.17	1.72e-07	4.18

Example 4.8: 2D acoustics with periodic boundary condition, subsonic background velocity. We consider the acoustic equations (3.16) with coefficients $\rho_0 = K_0 = 1$, and $u_0 = .5$, $v_0 = 0$, i.e.,

$$\begin{aligned} p_t + .5p_x + u_x + v_y &= 0, \\ u_t + .5u_x + p_x &= 0, \\ v_t + .5v_x + p_y &= 0, \end{aligned}$$

on a unit square $\Omega = [0, 1] \times [0, 1]$ with initial condition $p(x, y, 0) = \sin(2\pi(x + y))$, $u(x, 0) = v(x, 0) = 0$, and a periodic boundary condition. The exact solution is the following plane wave solution

$$\begin{aligned} p(x, y, t) &= \frac{1}{2} \sin(2\pi(x + y - (\sqrt{2} + .5)t)) + \frac{1}{2} \sin(2\pi(x + y + (\sqrt{2} - .5)t)), \\ u(x, y, t) &= \frac{\sqrt{2}}{4} \sin(2\pi(x + y - (\sqrt{2} + .5)t)) - \frac{\sqrt{2}}{4} \sin(2\pi(x + y + (\sqrt{2} - .5)t)), \\ v(x, y, t) &= \frac{\sqrt{2}}{4} \sin(2\pi(x + y - (\sqrt{2} + .5)t)) - \frac{\sqrt{2}}{4} \sin(2\pi(x + y + (\sqrt{2} - .5)t)). \end{aligned}$$

We present numerical results with the upwinding DG method (U), central DG method (C), the DG method (A) for the augmented 4-components system (3.18) in section 3.3.2, and also the DG method (A-Double) for the augmented 6-components system (3.11). The method (A-Double) is only tested for triangular meshes. Table 4.6 and Table 4.7 lists the numerical errors and their orders for the above DG methods at $T = 0.1$ on the non-uniform rectangular meshes, and triangular meshes, respectively. Again, we use Q^k/P^k polynomials with $1 \leq k \leq 3$.

From the tables, we observe optimal $(k+1)$ th order of accuracy for all the variable p_h , u_h , v_h , and ϕ_h for the 4-components energy-conserving DG method (A) on both types of meshes. We also observe optimal convergence for the 6-components, energy conserving DG method (A-Double) on triangular meshes, with a smaller absolute error compared with the method (A). The optimal convergence on rectangular meshes is understood; see Remark 3.4. But we do not have a theoretical proof for such optimality on the triangular meshes for both methods. We also observe optimal convergence for the method (U), but suboptimal convergence for the method (C) for all polynomial degrees.

Example 4.9: 2D acoustics, zero background velocity. We consider the acoustic equations (3.16) with coefficients $\rho_0 = K_0 = 1$, and $u_0 = 0$, $v_0 = 0$, i.e.,

$$\begin{aligned} p_t + u_x + v_y &= 0, \\ u_t + p_x &= 0, \\ v_t + p_y &= 0, \end{aligned}$$

on a unit square $\Omega = [0, 1] \times [0, 1]$ with initial condition $p(x, y, 0) = \sin(2\pi(x + y))$, $u(x, 0) = v(x, 0) = 0$, and a periodic boundary condition. The exact solution is

TABLE 4.6. The L^2 -errors and orders for Example 4.8 for the upwinding DG method (U), the central DG method (C), and the new DG method (A) on a non-uniform rectangular mesh with $N \times N$ cells. $T = 0.1$.

		(U)							
	N	$\ p - p_h\ $	Order	$\ u - u_h\ $	Order	$\ v - v_h\ $	Order		
P^1	10	1.22e-02	-0.00	1.40e-02	-0.00	1.40e-02	-0.00		
	20	3.34e-03	1.86	3.30e-03	2.08	3.57e-03	1.97		
	40	8.70e-04	1.94	7.98e-04	2.05	8.94e-04	2.00		
P^2	10	6.97e-04	-0.00	6.93e-04	-0.00	7.43e-04	-0.00		
	20	9.10e-05	2.94	8.40e-05	3.04	9.31e-05	3.00		
	40	1.16e-05	2.98	1.03e-05	3.03	1.16e-05	3.01		
P^3	10	2.84e-05	-0.00	2.74e-05	-0.00	2.94e-05	-0.00		
	20	1.85e-06	3.94	1.68e-06	4.03	1.88e-06	3.97		
	40	1.17e-07	3.98	1.04e-07	4.01	1.17e-07	4.01		
		(C)							
	N	$\ p - p_h\ $	Order	$\ u - u_h\ $	Order	$\ v - v_h\ $	Order		
P^1	10	2.93e-02	-0.00	8.09e-02	-0.00	3.52e-02	-0.00		
	20	1.39e-02	1.08	4.10e-02	0.98	1.71e-02	1.04		
	40	6.86e-03	1.02	2.05e-02	1.00	8.49e-03	1.01		
P^2	10	6.66e-04	-0.00	8.29e-03	-0.00	9.82e-04	-0.00		
	20	1.10e-04	2.60	1.54e-03	2.43	4.73e-04	1.05		
	40	1.76e-05	2.64	7.86e-05	4.29	1.18e-04	2.01		
P^3	10	6.52e-05	-0.00	2.62e-04	-0.00	7.97e-05	-0.00		
	20	8.10e-06	3.01	2.72e-05	3.27	8.55e-06	3.22		
	40	1.01e-06	3.01	2.68e-06	3.34	1.05e-06	3.03		
		(A)							
	N	$\ p - p_h\ $	Order	$\ u - u_h\ $	Order	$\ v - v_h\ $	Order	$\ \phi_h\ $	Order
P^1	10	2.14e-02	-0.00	3.24e-02	-0.00	1.40e-02	-0.00	4.39e-03	-0.00
	20	4.45e-03	2.27	8.10e-03	2.00	3.11e-03	2.17	1.80e-03	1.29
	40	1.05e-03	2.08	2.00e-03	2.01	7.42e-04	2.07	4.64e-04	1.95
P^2	10	9.88e-04	-0.00	1.66e-03	-0.00	7.31e-04	-0.00	2.95e-04	-0.00
	20	1.11e-04	3.16	2.01e-04	3.04	8.09e-05	3.18	5.15e-05	2.52
	40	1.36e-05	3.03	2.53e-05	2.99	9.51e-06	3.09	6.05e-06	3.09
P^3	10	3.63e-05	-0.00	6.39e-05	-0.00	2.61e-05	-0.00	1.51e-05	-0.00
	20	2.25e-06	4.02	4.06e-06	3.98	1.58e-06	4.04	8.94e-07	4.08
	40	1.38e-07	4.02	2.54e-07	4.00	9.70e-08	4.03	5.83e-08	3.94

the following plane wave solution

$$\begin{aligned}
 p(x, y, t) &= \frac{1}{2} \sin(2\pi(x + y - (\sqrt{2})t)) + \frac{1}{2} \sin(2\pi(x + y + (\sqrt{2})t)), \\
 u(x, y, t) &= \frac{\sqrt{2}}{4} \sin(2\pi(x + y - (\sqrt{2})t)) - \frac{\sqrt{2}}{4} \sin(2\pi(x + y + (\sqrt{2})t)), \\
 v(x, y, t) &= \frac{\sqrt{2}}{4} \sin(2\pi(x + y - (\sqrt{2})t)) - \frac{\sqrt{2}}{4} \sin(2\pi(x + y + (\sqrt{2})t)).
 \end{aligned}$$

TABLE 4.7. The L^2 -errors and orders for Example 4.8 for the upwinding DG method (U), the central DG method (C), the new DG method (A) (4-components), and the DG method (A-Double) (6-components) on a unstructured triangular mesh with mesh size $h = 1/N$. The scalar ϕ_h is the auxiliary variable for method (A), while the (3-components) vector ϕ_h is the auxiliary variable for method (A-Double). $T = 0.1$.

		(U)							
	N	$\ p - p_h\ $	Order	$\ u - u_h\ $	Order	$\ v - v_h\ $	Order		
P^1	10	9.88e-03	-0.00	1.16e-02	-0.00	1.00e-02	-0.00		
	20	2.65e-03	1.90	2.79e-03	2.05	2.60e-03	1.95		
	40	6.80e-04	1.96	6.85e-04	2.03	6.43e-04	2.02		
P^2	10	6.94e-04	-0.00	7.94e-04	-0.00	6.72e-04	-0.00		
	20	8.81e-05	2.98	1.02e-04	2.97	8.34e-05	3.01		
	40	1.07e-05	3.05	1.18e-05	3.11	9.94e-06	3.07		
P^3	10	3.75e-05	-0.00	4.29e-05	-0.00	3.63e-05	-0.00		
	20	2.38e-06	3.98	2.65e-06	4.02	2.32e-06	3.97		
	40	1.40e-07	4.08	1.50e-07	4.15	1.31e-07	4.14		
		(C)							
	N	$\ p - p_h\ $	Order	$\ u - u_h\ $	Order	$\ v - v_h\ $	Order		
P^1	10	3.11e-02	-0.00	2.10e-01	-0.00	6.07e-02	-0.00		
	20	1.58e-02	0.98	1.09e-01	0.95	2.84e-02	1.10		
	40	7.58e-03	1.06	5.66e-02	0.94	1.33e-02	1.09		
P^2	10	2.83e-03	-0.00	6.84e-03	-0.00	5.28e-03	-0.00		
	20	6.22e-04	2.18	1.34e-03	2.36	1.25e-03	2.08		
	40	1.50e-04	2.05	3.03e-04	2.14	2.65e-04	2.23		
P^3	10	1.62e-04	-0.00	8.24e-04	-0.00	2.94e-04	-0.00		
	20	1.82e-05	3.15	9.54e-05	3.11	3.24e-05	3.18		
	40	2.28e-06	3.00	8.38e-06	3.51	3.99e-06	3.02		
		(A)							
	N	$\ p - p_h\ $	Order	$\ u - u_h\ $	Order	$\ v - v_h\ $	Order	$\ \phi_h\ $	Order
P^1	10	1.51e-02	-0.00	1.73e-02	-0.00	1.35e-02	-0.00	1.48e-02	-0.00
	20	3.38e-03	2.16	4.55e-03	1.93	3.44e-03	1.97	3.58e-03	2.05
	40	8.26e-04	2.03	1.09e-03	2.07	7.29e-04	2.24	6.67e-04	2.42
P^2	10	9.38e-04	-0.00	1.35e-03	-0.00	1.02e-03	-0.00	1.10e-03	-0.00
	20	1.12e-04	3.06	1.76e-04	2.94	1.11e-04	3.20	1.31e-04	3.07
	40	1.30e-05	3.11	1.78e-05	3.30	1.13e-05	3.30	1.29e-05	3.34
P^3	10	5.07e-05	-0.00	6.36e-05	-0.00	5.06e-05	-0.00	6.19e-05	-0.00
	20	3.04e-06	4.06	4.19e-06	3.93	2.95e-06	4.10	3.09e-06	4.32
	40	1.68e-07	4.18	2.29e-07	4.19	1.51e-07	4.29	1.49e-07	4.38
		(A-Double)							
	N	$\ p - p_h\ $	Order	$\ u - u_h\ $	Order	$\ v - v_h\ $	Order	$\ \phi_h\ $	Order
P^1	10	7.76e-03	-0.00	7.94e-03	-0.00	6.96e-03	-0.00	1.41e-02	-0.00
	20	1.93e-03	2.01	2.09e-03	1.92	1.77e-03	1.98	3.43e-03	2.04
	40	4.79e-04	2.01	4.98e-04	2.07	4.35e-04	2.02	8.61e-04	1.99
P^2	10	5.08e-04	-0.00	5.81e-04	-0.00	5.11e-04	-0.00	8.80e-04	-0.00
	20	6.71e-05	2.92	7.03e-05	3.05	6.02e-05	3.09	1.12e-04	2.97
	40	7.99e-06	3.07	8.28e-06	3.09	7.28e-06	3.05	1.34e-05	3.07
P^3	10	2.85e-05	-0.00	3.03e-05	-0.00	2.48e-05	-0.00	5.17e-05	-0.00
	20	1.70e-06	4.07	1.98e-06	3.94	1.64e-06	3.92	3.12e-06	4.05
	40	9.87e-08	4.10	1.06e-07	4.22	9.24e-08	4.15	1.79e-07	4.12

Similar to the previous example, we present numerical results with the upwinding DG method (U), central DG method (C), and the 3-components DG method (A) with an alternating flux in section 3.3.2. We also present numerical results with the DG method (A-Double) for the augmented 6-components system (3.11) on triangular meshes.

Note that the DG method with an alternating numerical flux (A) on triangular meshes was observed to be suboptimal in [25] for the Maxwell's equation.

Table 4.8 and Table 4.9 lists the numerical errors and their orders with the above DG methods at $T = 0.1$ on rectangular, and triangular meshes, respectively. We use Q^k/P^k polynomials with $1 \leq k \leq 3$.

From the tables, while we still observe optimal $(k + 1)$ th order of accuracy for all the variable for method (A) on rectangular meshes, which is in agreement with Remark 3.4, we only get suboptimal convergence order of k for the velocity variables u_h and v_h on triangular meshes. On the other hand, the method (A-Double) is still optimally convergent on triangular meshes. Similar as the previous example, the method (U) is optimally convergent, but (C) is suboptimal.

Example 4.10: 2D elastodynamics with periodic boundary condition.

We consider the equations for elastodynamics (3.23) with coefficients $\lambda = 2, \mu = 1, \rho = 1$. The domain is a unit square $\Omega = [0, 1] \times [0, 1]$, and a periodic boundary condition is used. The initial condition is chosen such that exact solution is the following plane wave solution:

$$\begin{aligned}\sigma_{xx}(x, y, t) &= -\mu \sin(2\pi(x + y + \frac{\sqrt{2}}{2}c_s t)) + (\lambda + \mu) \sin(2\pi(x + y - \frac{\sqrt{2}}{2}c_p t)), \\ \sigma_{yy}(x, y, t) &= \mu \sin(2\pi(x + y + \frac{\sqrt{2}}{2}c_s t)) + (\lambda + \mu) \sin(2\pi(x + y - \frac{\sqrt{2}}{2}c_p t)), \\ \sigma_{xy}(x, y, t) &= \mu \sin(2\pi(x + y - \frac{\sqrt{2}}{2}c_p t)), \\ v(x, y, t) &= -\frac{\sqrt{2}}{2}c_s \sin(2\pi(x + y + \frac{\sqrt{2}}{2}c_s t)) - \frac{\sqrt{2}}{2}c_p \sin(2\pi(x + y - \frac{\sqrt{2}}{2}c_p t)), \\ w(x, y, t) &= \frac{\sqrt{2}}{2}c_s \sin(2\pi(x + y + \frac{\sqrt{2}}{2}c_s t)) - \frac{\sqrt{2}}{2}c_p \sin(2\pi(x + y - \frac{\sqrt{2}}{2}c_p t)),\end{aligned}$$

where $c_p = \sqrt{\frac{\lambda+2\mu}{\rho}}$ is the P wave speed, and $c_s = \sqrt{\frac{\mu}{\rho}}$ is the S wave speed.

Similar to the previous example, we present numerical results with the upwinding DG method (U), central DG method (C), and the 5-components DG method (A) with an alternating flux in section 3.3.5. We also present numerical results with the DG method (A-Double) for the augmented 10-components system (3.11) on triangular meshes.

The results are similar to Example 4.9. From the tables, while we still observe optimal $(k+1)$ th order of accuracy for all the variable for method (A) on rectangular meshes, which is in agreement with Remark 3.4, we only get suboptimal convergence order of k for the stress variables $\sigma_{xx,h}, \sigma_{yy,h}$ and $\sigma_{xy,h}$ on triangular meshes. On the other hand, the method (A-Double) is still optimally convergent. Similar as Example 4.9, the method (U) is optimally convergent, but (C) is suboptimal.

Example 4.11: long time simulation: advection of a plane wave. We consider the advection equation (4.2) on the unit square with periodic boundary

TABLE 4.8. The L^2 -errors and orders for Example 4.9 for the upwinding DG method (U), the central DG method (C), and the new DG method (A) on a non-uniform rectangular mesh with $N \times N$ cells. $T = 0.1$.

		(U)					
	N	$\ p - p_h\ $	Order	$\ u - u_h\ $	Order	$\ v - v_h\ $	Order
P^1	10	1.25e-02	-0.00	1.37e-02	-0.00	1.37e-02	-0.00
	20	3.37e-03	1.89	3.21e-03	2.10	3.22e-03	2.09
	40	8.71e-04	1.95	7.77e-04	2.05	7.78e-04	2.05
P^2	10	7.08e-04	-0.00	6.92e-04	-0.00	6.91e-04	-0.00
	20	9.12e-05	2.96	8.20e-05	3.08	8.24e-05	3.07
	40	1.16e-05	2.98	1.01e-05	3.02	1.01e-05	3.03
P^3	10	2.86e-05	-0.00	2.68e-05	-0.00	2.66e-05	-0.00
	20	1.86e-06	3.94	1.64e-06	4.03	1.65e-06	4.01
	40	1.17e-07	3.98	1.02e-07	4.01	1.02e-07	4.02
		(C)					
	N	$\ p - p_h\ $	Order	$\ u - u_h\ $	Order	$\ v - v_h\ $	Order
P^1	10	2.99e-02	-0.00	2.73e-01	-0.00	2.73e-01	-0.00
	20	1.41e-02	1.08	1.39e-01	0.98	1.39e-01	0.98
	40	6.95e-03	1.02	6.96e-02	1.00	6.96e-02	0.99
P^2	10	6.54e-04	-0.00	8.70e-03	-0.00	2.25e-03	-0.00
	20	1.08e-04	2.60	1.59e-03	2.45	1.51e-03	0.58
	40	1.77e-05	2.61	1.17e-04	3.76	3.77e-04	2.00
P^3	10	5.84e-05	-0.00	5.79e-04	-0.00	5.57e-04	-0.00
	20	7.22e-06	3.02	7.13e-05	3.02	6.90e-05	3.01
	40	9.06e-07	2.99	8.68e-06	3.04	8.67e-06	2.99
		(A)					
	N	$\ p - p_h\ $	Order	$\ u - u_h\ $	Order	$\ v - v_h\ $	Order
P^1	10	1.52e-02	-0.00	9.27e-02	-0.00	9.25e-02	-0.00
	20	3.88e-03	1.97	2.37e-02	1.97	2.36e-02	1.97
	40	9.74e-04	1.99	5.95e-03	2.00	5.94e-03	1.99
P^2	10	7.90e-04	-0.00	4.71e-03	-0.00	4.72e-03	-0.00
	20	1.01e-04	2.97	6.01e-04	2.97	5.96e-04	2.98
	40	1.27e-05	2.99	7.49e-05	3.00	7.49e-05	2.99
P^3	10	3.15e-05	-0.00	1.85e-04	-0.00	1.87e-04	-0.00
	20	2.03e-06	3.95	1.19e-05	3.95	1.18e-05	3.99
	40	1.27e-07	4.00	7.43e-07	4.01	7.43e-07	3.99

condition and initial condition $u(x, y, 0) = \sin(4\pi(x+y))$. This is a two dimensional extension of the test Example 4.4. We present numerical results for the three P^2 -DG methods, (U) for upwinding flux, (C) for central flux, and (A) for the new method. Both uniform rectangular mesh and unstructured triangular mesh are considered. We use the RK3 time stepping. The CFL number is taken to be 0.05 on the rectangular mesh, and 0.02 on the triangular mesh.

Numerical results on the cut line $y = .5$ at time $T = 40$ (wave propagates 80 cycles) are shown in Figure 8. Figure 8 indicates the superior performance of the new method on both rectangular and triangular meshes over the dissipative

TABLE 4.9. The L^2 -errors and orders for Example 4.9 for the upwinding DG method (U), the central DG method (C), the alternating flux DG method (A), and the DG method (A-Double) (6-components) on a unstructured triangular mesh with mesh size $h = 1/N$. $T = 0.1$.

		(U)					
	N	$\ p - p_h\ $	Order	$\ u - u_h\ $	Order	$\ v - v_h\ $	Order
P^1	10	9.24e-03	-0.00	1.90e-02	-0.00	2.16e-02	-0.00
	20	2.41e-03	1.94	4.11e-03	2.21	4.23e-03	2.35
	40	6.11e-04	1.98	8.68e-04	2.24	9.03e-04	2.23
P^2	10	6.29e-04	-0.00	8.04e-04	-0.00	8.15e-04	-0.00
	20	8.20e-05	2.94	9.12e-05	3.14	9.17e-05	3.15
	40	1.00e-05	3.04	1.03e-05	3.14	1.07e-05	3.10
P^3	10	3.44e-05	-0.00	3.97e-05	-0.00	3.83e-05	-0.00
	20	2.12e-06	4.02	2.39e-06	4.05	2.39e-06	4.00
	40	1.25e-07	4.09	1.33e-07	4.17	1.36e-07	4.14
		(C)					
	N	$\ p - p_h\ $	Order	$\ u - u_h\ $	Order	$\ v - v_h\ $	Order
P^1	10	1.49e-02	-0.00	6.14e-01	-0.00	6.12e-01	-0.00
	20	3.88e-03	1.94	3.14e-01	0.97	3.17e-01	0.95
	40	9.50e-04	2.03	1.55e-01	1.02	1.57e-01	1.02
P^2	10	7.09e-04	-0.00	3.61e-02	-0.00	3.62e-02	-0.00
	20	8.62e-05	3.04	9.41e-03	1.94	9.58e-03	1.92
	40	1.00e-05	3.10	2.19e-03	2.11	2.29e-03	2.06
P^3	10	4.21e-05	-0.00	3.75e-03	-0.00	3.77e-03	-0.00
	20	3.48e-06	3.60	4.71e-04	2.99	4.76e-04	2.99
	40	3.74e-07	3.22	5.69e-05	3.05	5.77e-05	3.04
		(A)					
	N	$\ p - p_h\ $	Order	$\ u - u_h\ $	Order	$\ v - v_h\ $	Order
P^1	10	1.15e-02	-0.00	2.48e-01	-0.00	2.05e-01	-0.00
	20	2.88e-03	1.99	1.40e-01	0.83	1.15e-01	0.83
	40	7.15e-04	2.01	5.57e-02	1.33	6.66e-02	0.79
P^2	10	7.07e-04	-0.00	2.21e-02	-0.00	2.47e-02	-0.00
	20	9.57e-05	2.88	6.53e-03	1.76	6.28e-03	1.97
	40	1.14e-05	3.07	1.43e-03	2.19	1.65e-03	1.93
P^3	10	3.97e-05	-0.00	2.03e-03	-0.00	1.54e-03	-0.00
	20	2.32e-06	4.09	2.62e-04	2.95	2.21e-04	2.80
	40	1.38e-07	4.08	2.50e-05	3.39	2.95e-05	2.91
		(A-Double)					
	N	$\ p - p_h\ $	Order	$\ u - u_h\ $	Order	$\ v - v_h\ $	Order
P^1	10	7.67e-03	-0.00	1.75e-02	-0.00	2.02e-02	-0.00
	20	1.91e-03	2.00	3.81e-03	2.20	3.81e-03	2.41
	40	4.77e-04	2.00	7.83e-04	2.28	7.91e-04	2.27
P^2	10	5.03e-04	-0.00	6.49e-04	-0.00	6.62e-04	-0.00
	20	6.77e-05	2.89	6.67e-05	3.28	6.90e-05	3.26
	40	8.01e-06	3.08	7.81e-06	3.09	8.11e-06	3.09
P^3	10	2.82e-05	-0.00	2.97e-05	-0.00	2.81e-05	-0.00
	20	1.66e-06	4.09	1.91e-06	3.96	1.91e-06	3.88
	40	9.78e-08	4.08	1.03e-07	4.21	1.07e-07	4.16

TABLE 4.10. The L^2 -errors and orders for Example 4.10 for the methods (U), (C), and (A) on a non-uniform rectangular mesh with $N \times N$ cells. The stress errors $e_s^1 = \|\sigma_{xx} - \sigma_{xx,h}\|$, $e_s^2 = \|\sigma_{yy} - \sigma_{yy,h}\|$, $e_s^3 = \|\sigma_{xy} - \sigma_{xy,h}\|$, and the velocity error $e_v = \sqrt{\|v - v_h\|^2 + \|w - w_h\|^2}$ are recorded. $T = 0.1$.

		(U)							
	N	e_s^1	Order	e_s^2	Order	e_s^3	Order	e_v	Order
P^1	10	7.66e-02	-0.00	6.70e-02	-0.00	3.80e-02	-0.00	4.66e-02	-0.00
	20	2.04e-02	1.91	1.82e-02	1.88	7.07e-03	2.43	1.18e-02	1.98
	40	5.50e-03	1.89	4.62e-03	1.98	1.50e-03	2.23	2.96e-03	2.00
P^2	10	1.16e-02	-0.00	9.58e-03	-0.00	3.45e-03	-0.00	3.03e-03	-0.00
	20	1.81e-03	2.67	1.66e-03	2.53	4.11e-04	3.07	3.95e-04	2.94
	40	2.87e-04	2.66	2.75e-04	2.59	5.01e-05	3.04	4.96e-05	2.99
P^3	10	2.73e-04	-0.00	2.22e-04	-0.00	5.84e-05	-0.00	1.02e-04	-0.00
	20	1.93e-05	3.83	1.59e-05	3.80	3.50e-06	4.06	6.42e-06	3.98
	40	1.31e-06	3.87	9.93e-07	4.00	2.03e-07	4.11	4.01e-07	4.00
		(C)							
	N	e_s^1	Order	e_s^2	Order	e_s^3	Order	e_v	Order
P^1	10	1.66e+00	-0.00	1.06e+00	-0.00	6.35e-01	-0.00	8.58e-02	-0.00
	20	8.48e-01	0.97	5.32e-01	0.99	3.12e-01	1.02	4.08e-02	1.07
	40	4.26e-01	0.99	2.67e-01	1.00	1.55e-01	1.01	2.02e-02	1.02
P^2	10	5.37e-02	-0.00	6.01e-03	-0.00	4.75e-03	-0.00	3.94e-03	-0.00
	20	9.82e-03	2.45	3.11e-03	0.95	1.23e-03	1.95	9.72e-04	2.02
	40	7.38e-04	3.73	7.54e-04	2.05	2.63e-04	2.23	1.90e-04	2.35
P^3	10	3.68e-03	-0.00	1.62e-03	-0.00	6.47e-04	-0.00	2.76e-04	-0.00
	20	4.55e-04	3.01	2.05e-04	2.98	8.14e-05	2.99	3.46e-05	3.00
	40	5.56e-05	3.03	2.59e-05	2.99	1.01e-05	3.01	4.27e-06	3.01
		(A)							
	N	e_s^1	Order	e_s^2	Order	e_s^3	Order	e_v	Order
P^1	10	5.57e-01	-0.00	1.84e-01	-0.00	5.32e-02	-0.00	6.62e-02	-0.00
	20	1.44e-01	1.95	4.30e-02	2.10	8.53e-03	2.64	1.49e-02	2.15
	40	3.63e-02	1.99	1.06e-02	2.02	1.68e-03	2.34	3.54e-03	2.08
P^2	10	2.82e-02	-0.00	8.66e-03	-0.00	2.69e-03	-0.00	3.33e-03	-0.00
	20	3.65e-03	2.95	1.07e-03	3.01	2.38e-04	3.50	3.68e-04	3.18
	40	4.57e-04	3.00	1.34e-04	3.00	2.26e-05	3.39	4.50e-05	3.03
P^3	10	1.12e-03	-0.00	3.37e-04	-0.00	8.05e-05	-0.00	1.19e-04	-0.00
	20	7.27e-05	3.95	2.11e-05	4.00	3.85e-06	4.39	7.42e-06	4.00
	40	4.53e-06	4.00	1.33e-06	3.99	2.13e-07	4.18	4.57e-07	4.02

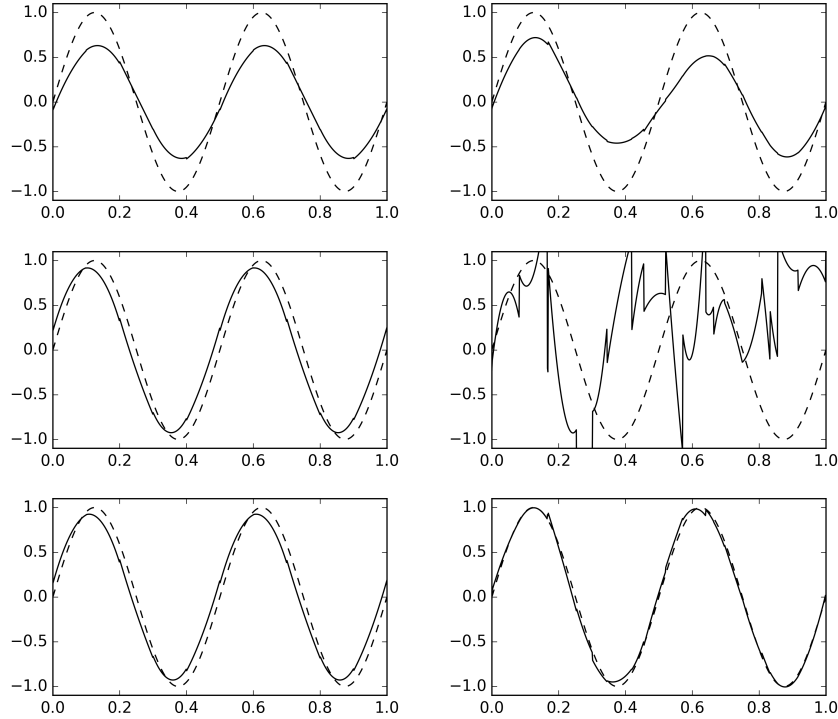
upwinding DG method. The results on the rectangular mesh for the central DG method and the new methods are comparable, both have small dissipation error with a slight phase shift. However, the result on triangular mesh for the new method is clearly better than the central DG method, which is very oscillatory.

Example 4.12: long time simulation: advection of a Gaussian pulse. We consider the advection equation (4.2) on the unit square with periodic boundary condition and initial condition $u(x, y, 0) = \exp(-200((x - 0.5)^2 + (y - .5)^2))$. This

TABLE 4.11. The L^2 -errors and orders for Example 4.10 for the methods (U), (C), (A), and (A-Double) on a triangular mesh with mesh size $h = 1/N$. The stress errors $e_s^1 = \|\sigma_{xx} - \sigma_{xx,h}\|$, $e_s^2 = \|\sigma_{yy} - \sigma_{yy,h}\|$, $e_s^3 = \|\sigma_{xy} - \sigma_{xy,h}\|$, and the velocity error $e_v = \sqrt{\|v - v_h\|^2 + \|w - w_h\|^2}$ are recorded. $T = 0.1$.

		(U)							
	N	e_s^1	Order	e_s^2	Order	e_s^3	Order	e_v	Order
P^1	10	6.12e-02	-0.00	5.71e-02	-0.00	2.66e-02	-0.00	3.79e-02	-0.00
	20	1.57e-02	1.97	1.42e-02	2.00	6.15e-03	2.11	9.85e-03	1.94
	40	3.84e-03	2.03	3.52e-03	2.02	1.43e-03	2.10	2.42e-03	2.02
P^2	10	5.80e-03	-0.00	6.13e-03	-0.00	2.86e-03	-0.00	2.81e-03	-0.00
	20	9.28e-04	2.64	1.05e-03	2.55	5.93e-04	2.27	3.46e-04	3.02
	40	1.22e-04	2.93	1.46e-04	2.84	8.09e-05	2.87	4.23e-05	3.03
P^3	10	2.98e-04	-0.00	3.39e-04	-0.00	1.64e-04	-0.00	1.33e-04	-0.00
	20	1.80e-05	4.05	2.32e-05	3.87	9.79e-06	4.06	8.91e-06	3.90
	40	1.11e-06	4.01	1.53e-06	3.92	6.18e-07	3.99	4.97e-07	4.16
		(C)							
	N	e_s^1	Order	e_s^2	Order	e_s^3	Order	e_v	Order
P^1	10	3.10e+00	-0.00	1.59e+00	-0.00	1.63e+00	-0.00	5.32e-02	-0.00
	20	1.50e+00	1.05	6.65e-01	1.26	8.35e-01	0.97	1.15e-02	2.21
	40	7.37e-01	1.02	3.11e-01	1.09	4.07e-01	1.04	2.81e-03	2.04
P^2	10	1.22e-01	-0.00	9.32e-02	-0.00	9.13e-02	-0.00	3.34e-03	-0.00
	20	2.69e-02	2.19	2.30e-02	2.02	2.28e-02	2.00	3.41e-04	3.29
	40	5.55e-03	2.28	5.32e-03	2.11	5.04e-03	2.18	4.00e-05	3.09
P^3	10	1.94e-02	-0.00	1.09e-02	-0.00	1.01e-02	-0.00	2.09e-04	-0.00
	20	2.29e-03	3.08	1.09e-03	3.33	1.26e-03	3.01	1.73e-05	3.60
	40	2.76e-04	3.05	1.30e-04	3.07	1.50e-04	3.07	1.55e-06	3.48
		(A)							
	N	e_s^1	Order	e_s^2	Order	e_s^3	Order	e_v	Order
P^1	10	1.14e+00	-0.00	3.62e-01	-0.00	4.08e-01	-0.00	4.22e-02	-0.00
	20	6.69e-01	0.77	2.27e-01	0.67	2.31e-01	0.82	1.08e-02	1.97
	40	2.21e-01	1.60	1.29e-01	0.81	1.06e-01	1.12	2.63e-03	2.04
P^2	10	9.88e-02	-0.00	3.72e-02	-0.00	3.99e-02	-0.00	2.88e-03	-0.00
	20	3.06e-02	1.69	1.21e-02	1.62	1.13e-02	1.82	3.47e-04	3.05
	40	6.16e-03	2.31	3.32e-03	1.87	2.80e-03	2.01	4.11e-05	3.08
P^3	10	1.02e-02	-0.00	2.83e-03	-0.00	2.96e-03	-0.00	1.39e-04	-0.00
	20	1.27e-03	3.00	4.71e-04	2.59	4.18e-04	2.82	9.35e-06	3.90
	40	1.03e-04	3.63	6.43e-05	2.88	4.98e-05	3.07	5.22e-07	4.16
		(A-Double)							
	N	e_s^1	Order	e_s^2	Order	e_s^3	Order	e_v	Order
P^1	10	7.65e-02	-0.00	5.76e-02	-0.00	3.86e-02	-0.00	2.73e-02	-0.00
	20	1.98e-02	1.95	1.62e-02	1.83	9.72e-03	1.99	6.99e-03	1.96
	40	4.79e-03	2.05	4.01e-03	2.01	2.31e-03	2.07	1.71e-03	2.03
P^2	10	9.88e-02	-0.00	3.72e-02	-0.00	3.99e-02	-0.00	2.88e-03	-0.00
	20	3.06e-02	1.69	1.21e-02	1.62	1.13e-02	1.82	3.47e-04	3.05
	40	6.16e-03	2.31	3.32e-03	1.87	2.80e-03	2.01	4.11e-05	3.08
P^3	10	2.03e-04	-0.00	1.26e-04	-0.00	7.98e-05	-0.00	9.67e-05	-0.00
	20	1.35e-05	3.91	8.59e-06	3.88	5.43e-06	3.88	6.46e-06	3.90
	40	7.43e-07	4.19	4.95e-07	4.12	3.15e-07	4.11	3.60e-07	4.17

FIGURE 8. Numerical solution at $T = 40$ on the cut line $y = 0.5$ for Example 4.11. RK3 time stepping. Top row: method (U). Middle row: method (C). Bottom row: method (A). Left: square mesh with 10×10 cells, Q^2 space. Right: triangular mesh with meshsize $h = 0.1$, P^2 space. (Roughly 15 dofs/wavelength in each direction)

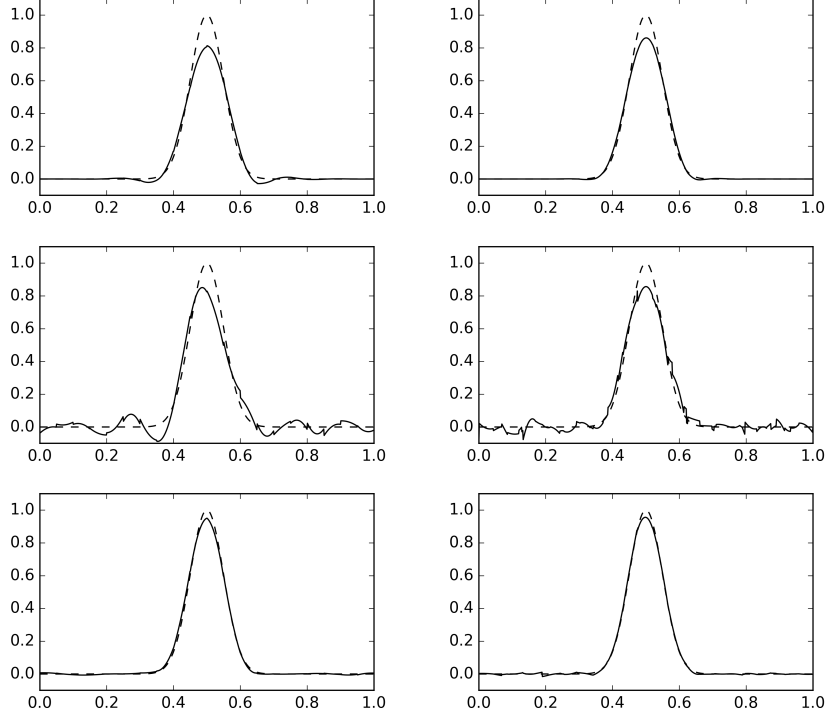


is a two dimensional analog of the test Example 4.5. We present numerical results for the three DG methods using Q^2/P^2 space. Both uniform rectangular mesh and unstructured triangular mesh are considered. We use the RK3 time stepping. The CFL number is taken to be 0.05 on the rectangular mesh, and 0.02 on the triangular mesh.

Numerical results on the cut line $y = .5$ at time $T = 10$ (wave propagates 10 cycles) are shown in Figure 9. Figure 9 indicates the superior performance of the new method on both rectangular and triangular meshes over the dissipative upwinding DG method in terms of dissipation error. It is also superior over the central DG method in terms of both dissipation and dispersion error.

Example 4.13: long time simulation: 2D acoustics with time periodic source. We consider the following acoustic equations on the whole space \mathbb{R}^2 with

FIGURE 9. Numerical solution at $T = 10$ on the cut line $y = 0.5$ for Example 4.12. RK3 time stepping. Top row: method (U). Middle row: method (C). Bottom row: method (A). Left: square mesh with 20×20 cells, Q^2 space. Right: triangular mesh with meshsize $h = 0.05$, P^2 space. (Roughly 60 dofs in each direction)



time periodic source:

$$\begin{aligned} p_t + u_x + v_y &= S, \\ u_t + p_x &= 0, \\ v_t + p_y &= 0, \end{aligned}$$

where the source term

$$S = \exp \left[-\ln(2) \left(\frac{x^2 + y^2}{(0.2)^2} \right) \right] \sin(\omega t), \quad \text{with } \omega = 4\pi.$$

Zero initial condition is considered. The exact solution to the above equations can be found in [27]. We specifically mention that, the exact solution $p(x, y, t)$ is purely radial, with its spatial dependence only through the radius $r = \sqrt{x^2 + y^2}$, and at any physical location (x, y) , it is 0 (at rest) for $t < r$, and is time-periodic with frequency $\omega = 4\pi$ for $t > r$.

We shall consider the numerical solution on a stretched rectangular domain

$$\Omega = [0, 12] \times [0, 1].$$

The final time of the simulation is $T = 10$.

The boundary treatment is given as follows. By symmetry of the problem, the symmetry (wall) boundary condition is used along the left ($x = 0$) and bottom ($y = 0$) boundaries:

$$\begin{aligned}\widehat{\mathbf{B}_n \mathbf{u}_h} &= [0, p, 0]' && \text{on left boundary } x = 0, \\ \widehat{\mathbf{B}_n \mathbf{u}_h} &= [0, 0, p]' && \text{on bottom boundary } y = 0.\end{aligned}$$

At time $T = 10$, the solution is still at rest on the right boundary ($x = 12$), and a simple outflow boundary condition is imposed there. To treat the top boundary ($y = 1$), we impose a perfectly matched layer (PML) [22] with thickness 0.5,

$$\Omega_{pml} = [0, 12] \times [1, 1.5].$$

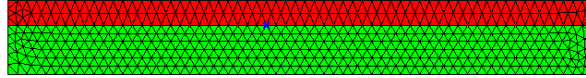
We solve the following PML-ODE system from [22] on the PML domain Ω_{pml} :

$$\begin{aligned}p_t + u_x + v_y &= -\sigma p, \\ u_t + p_x &= \sigma(u + \tilde{u}), \\ v_t + p_y &= -\sigma v, \\ \tilde{u}_t &= -\sigma(u + \tilde{u}),\end{aligned}$$

with the absorption constant σ taken to be $\sigma = 10$.

We present numerical results for the three DG methods with P^2 space on, (U) for upwinding flux, (C) for central flux, and (A) for the alternating flux. The RK3 time stepping is used, and CFL number is taken to be 0.05. We use a triangular mesh with mesh size $h = 0.2$, see Figure 10.

FIGURE 10. Computational mesh for Example 4.13. The PML region Ω_{pml} is colored in red, and the domain Ω is colored in green.

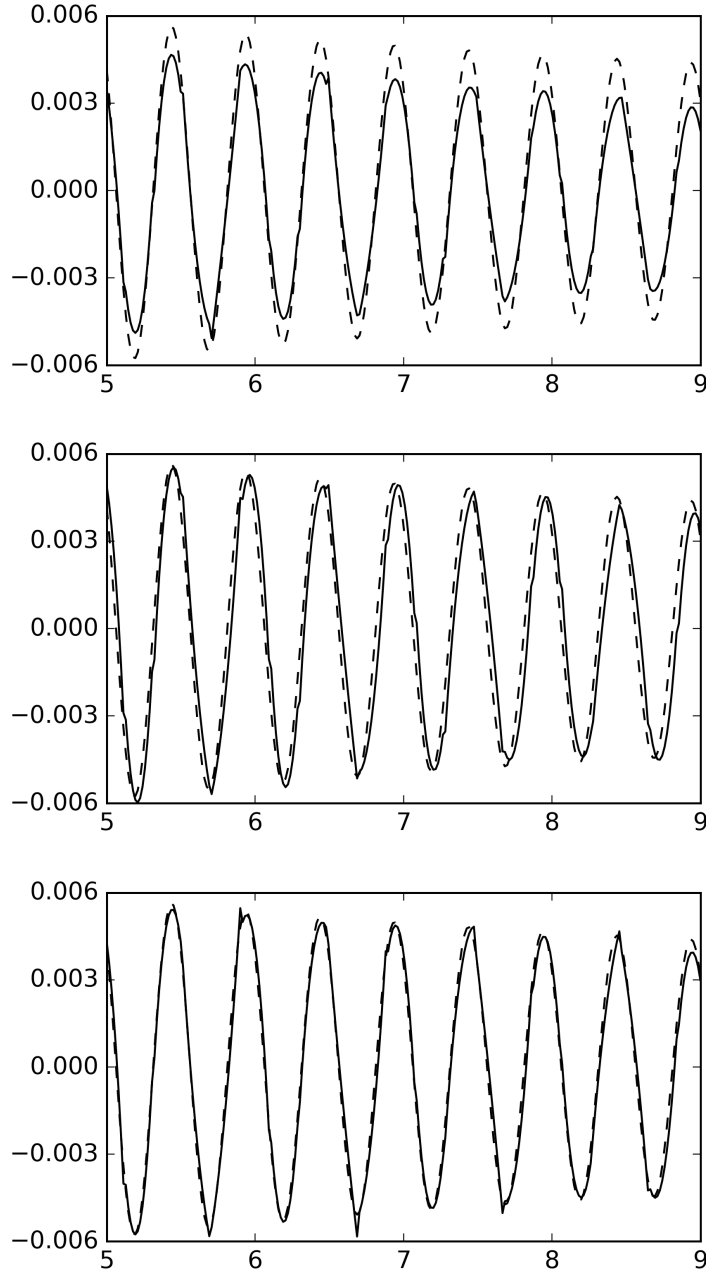


y
 x

Netgen 6.2-dev

Numerical results for the pressure field p_h on the segment $5 \leq x \leq 9$ along the x -axis are shown in Figure 11. The method (U) produce visible dissipation error, while the method (C) produce slight phase shift. The method (A) is better than (U) in terms of dissipation error, and better than (C) in terms of phase shift.

FIGURE 11. Pressure field at $T = 10$ on the segment $\{(x, 0) : 5 \leq x \leq 9\}$ for Example 4.14. RK3 time stepping. Top: method (U). Middle: method (C). Bottom: method (A). Solid line: numerical solution. Dashed line: exact solution.



5. CONCLUDING REMARKS

In this paper, we have proposed an energy conserving DG method for linear symmetric hyperbolic systems. The method is proven to be optimal convergent in one-space dimension, and in multi-space dimension on rectangular meshes.

Extensive numerical results are presented to assess the proposed method. In particular, we observe the optimal L^2 -convergence of the method in one-space dimension, and in two-space dimension using rectangular meshes. We also observe the optimal convergence of the method (with the doubling unknowns approach) on triangular meshes for all the tests considered in this paper. Numerical comparison of the new method with the DG methods using upwinding numerical fluxes, and central numerical fluxes for long time simulations are also presented. The new method is found to be better than the upwinding DG method in terms of the dissipation error, and to be better than the central DG method in terms of the dispersion error for all the numerical tests conducted in this paper.

REFERENCES

- [1] S. ABARBANEL AND D. GOTTLIEB, *Stability of two-dimensional initial-boundary value problems using leap-frog type schemes*, Math. Comp., 33 (1979), pp. 1145–1155.
- [2] J. L. BONA, H. CHEN, O. KARAKASHIAN, AND Y. XING, *Conservative, discontinuous Galerkin-methods for the generalized Korteweg-de Vries equation*, Math. Comp., 82 (2013), pp. 1401–1432.
- [3] M. H. CARPENTER, D. GOTTLIEB, S. ABARBANEL, AND W. S. DON, *The theoretical accuracy of Runge-Kutta time discretizations for the initial-boundary value problem: a study of the boundary error*, SIAM J. Sci. Comput., 16 (1995), pp. 1241–1252.
- [4] Y. CHEN, B. COCKBURN, AND B. DONG, *A new discontinuous Galerkin method, conserving the discrete H^2 -norm, for third-order linear equations in one space dimension*, IMA J. Numer. Anal., 36 (2016), pp. 1570–1598.
- [5] C.-S. CHOU, C.-W. SHU, AND Y. XING, *Optimal energy conserving local discontinuous Galerkin methods for second-order wave equation in heterogeneous media*, J. Comput. Phys., 272 (2014), pp. 88–107.
- [6] E. T. CHUNG AND B. ENQUIST, *Optimal discontinuous Galerkin methods for the acoustic wave equation in higher dimensions*, SIAM J. Numer. Anal., 47 (2009), pp. 3820–3848.
- [7] B. COCKBURN, G. KANSCHAT, I. PERUGIA, AND D. SCHÖTZAU, *Superconvergence of the local discontinuous Galerkin method for elliptic problems on Cartesian grids*, SIAM J. Numer. Anal., 39 (2001), pp. 264–285.
- [8] B. COCKBURN, G. E. KARNIADAKIS, AND C.-W. SHU, *The development of discontinuous Galerkin methods*, in Discontinuous Galerkin methods (Newport, RI, 1999), vol. 11 of Lect. Notes Comput. Sci. Eng., Springer, Berlin, 2000, pp. 3–50.
- [9] B. COCKBURN AND C.-W. SHU, *The local discontinuous Galerkin method for time-dependent convection-diffusion systems*, SIAM J. Numer. Anal., 35 (1998), pp. 2440–2463 (electronic).
- [10] ———, *Runge-Kutta discontinuous Galerkin methods for convection-dominated problems*, J. Sci. Comput., 16 (2001), pp. 173–261.
- [11] D. R. DURRAN, *Numerical methods for wave equations in geophysical fluid dynamics*, vol. 32 of Texts in Applied Mathematics, Springer-Verlag, New York, 1999.
- [12] R. S. FALK AND G. R. RICHTER, *Explicit finite element methods for linear hyperbolic systems*, in Discontinuous Galerkin methods (Newport, RI, 1999), vol. 11 of Lect. Notes Comput. Sci. Eng., Springer, Berlin, 2000, pp. 209–219.
- [13] L. FEZOU, S. LANTERI, S. LOHRENGEL, AND S. PIPERNO, *Convergence and stability of a discontinuous Galerkin time-domain method for the 3D heterogeneous Maxwell equations on unstructured meshes*, M2AN Math. Model. Numer. Anal., 39 (2005), pp. 1149–1176.
- [14] W. GUO, J.-M. QIU, AND J. QIU, *A new Lax-Wendroff discontinuous Galerkin method with superconvergence*, J. Sci. Comput., 65 (2015), pp. 299–326.
- [15] J. C. HARDIN, J. R. RISTORCELLI, AND C. TAM, *ICASE/LaRC workshop on Benchmark Problems in Computational Aeroacoustics.*, NASA CP 3300, 1995.

- [16] J. S. HESTHAVEN AND T. WARBURTON, *Nodal high-order methods on unstructured grids. I. Time-domain solution of Maxwell's equations*, J. Comput. Phys., 181 (2002), pp. 186–221.
- [17] N. A. KAMPANIS, J. EKATERINARIS, AND V. DOUGALIS, *Effective Computational Methods for Wave Propagation*, Chapman& Hall/CRC, 2008.
- [18] P. LASAINT AND P.-A. RAVIART, *On a finite element method for solving the neutron transport equation*, (1974), pp. 89–123. Publication No. 33.
- [19] P. LAX AND B. WENDROFF, *Systems of conservation laws*, Comm. Pure Appl. Math., 13 (1960), pp. 217–237.
- [20] R. J. LEVEQUE, *Finite volume methods for hyperbolic problems*, Cambridge Texts in Applied Mathematics, Cambridge University Press, Cambridge, 2002.
- [21] J. LI, C. SHI, AND C.-W. SHU, *Optimal non-dissipative discontinuous Galerkin methods for Maxwell's equations in Drude metamaterials*, Comput. Math. Appl., 73 (2017), pp. 1760–1780.
- [22] A. MODAVE, J. LAMBRECHTS, AND C. GEUZAIN, *Perfectly matched layers for convex truncated domains with discontinuous Galerkin time domain simulations*, Comput. Math. Appl., 73 (2017), pp. 684–700.
- [23] P. MONK AND G. R. RICHTER, *A discontinuous Galerkin method for linear symmetric hyperbolic systems in inhomogeneous media*, J. Sci. Comput., 22/23 (2005), pp. 443–477.
- [24] J. SCHÖBERL, *C++11 Implementation of Finite Elements in NGSolve*, 2014. ASC Report 30/2014, Institute for Analysis and Scientific Computing, Vienna University of Technology.
- [25] C. SHI, J. LI, AND C.-W. SHU, *Discontinuous Galerkin methods for Maxwell's equations in Drude metamaterials on unstructured meshes*, J. Comput. Appl. Math., to appear.
- [26] Z. SUN AND C.-W. SHU, *Stability analysis and error estimates of Lax-Wendroff discontinuous Galerkin methods for linear conservation laws*, ESAIM Math. Model. Numer. Anal., 51 (2017), pp. 1063–1087.
- [27] C. TAM AND J. HARDIN, *Second Computational Aeroacoustics (CAA) Workshop on Benchmark Problems*, NASA CP 3352, 1996.
- [28] Y. XING, C.-S. CHOU, AND C.-W. SHU, *Energy conserving local discontinuous Galerkin methods for wave propagation problems*, Inverse Probl. Imaging, 7 (2013), pp. 967–986.

DIVISION OF APPLIED MATHEMATICS, BROWN UNIVERSITY, PROVIDENCE, RI 02912
E-mail address: `guosheng_fu@brown.edu`

DIVISION OF APPLIED MATHEMATICS, BROWN UNIVERSITY, PROVIDENCE, RI 02912
E-mail address: `shu@dam.brown.edu`